10706–10725 *Nucleic Acids Research, 2017, Vol. 45, No. 18* *Published online 7 September 2017*
doi: 10.1093/nar/gkx786

Nuclear poly(A) binding protein 1 (PABPN1) and Matrin3 interact in muscle cells and regulate RNA processing

Ayan Banerjee[1], Katherine E. Vest[2], Grace K. Pavlath[2,*] and Anita H. Corbett[1,*]

[1]Department of Biology, Emory University, Atlanta, GA 30322, USA and [2]Department of Pharmacology, Emory University School of Medicine, Atlanta, GA 30322, USA

Received June 29, 2017; Revised August 18, 2017; Editorial Decision August 24, 2017; Accepted August 27, 2017

ABSTRACT

The polyadenylate binding protein 1 (PABPN1) is a ubiquitously expressed RNA binding protein vital for multiple steps in RNA metabolism. Although PABPN1 plays a critical role in the regulation of RNA processing, mutation of the gene encoding this ubiquitously expressed RNA binding protein causes a specific form of muscular dystrophy termed oculopharyngeal muscular dystrophy (OPMD). Despite the tissue-specific pathology that occurs in this disease, only recently have studies of PABPN1 begun to explore the role of this protein in skeletal muscle. We have used co-immunoprecipitation and mass spectrometry to identify proteins that interact with PABPN1 in mouse skeletal muscles. Among the interacting proteins we identified Matrin 3 (MATR3) as a novel protein interactor of PABPN1. The *MATR3* gene is mutated in a form of distal myopathy and amyotrophic lateral sclerosis (ALS). We demonstrate, that like PABPN1, MATR3 is critical for myogenesis. Furthermore, MATR3 controls critical aspects of RNA processing including alternative polyadenylation and intron retention. We provide evidence that MATR3 also binds and regulates the levels of long non-coding RNA (lncRNA) *Neat1* and together with PABPN1 is required for normal paraspeckle function. We demonstrate that PABPN1 and MATR3 are required for paraspeckles, as well as for adenosine to inosine (A to I) RNA editing of *Ctn* RNA in muscle cells. We provide a functional link between PABPN1 and MATR3 through regulation of a common lncRNA target with downstream impact on paraspeckle morphology and function. We extend our analysis to a mouse model of OPMD and demonstrate altered paraspeckle morphology in the presence of endogenous levels of alanine-expanded PABPN1. In this study, we report protein-binding partners of PABPN1, which could provide insight into novel functions of PABPN1 in skeletal muscle and identify proteins that could be sequestered with alanine-expanded PABPN1 in the nuclear aggregates found in OPMD.

INTRODUCTION

RNA binding proteins play essential roles in every step of gene expression from the regulation of highly coordinated co-transcriptional events in the nucleus such as splicing and polyadenylation to the translation and eventual decay of transcripts in the cytoplasm. Given the critical role of RNA binding proteins in gene expression, why mutations in genes that encode many of these ubiquitously expressed proteins cause tissue-specific diseases is unknown. While such mutations often cause neurological disease (1–3), they are also linked to the pathogenesis of muscular dystrophies such as myotonic dystrophy (4) and oculopharyngeal muscular dystrophy (OPMD) (5). OPMD is caused by mutation of the *PABPN1* gene which encodes the ubiquitously expressed poly (A) RNA binding protein nuclear 1 (PABPN1) (5).

The original function ascribed to PABPN1 is enhancing the processivity of poly (A) polymerase to regulate poly (A) tail length (6–9). However, recent studies have identified roles for PABPN1 in a number of additional post-transcriptional regulatory processes including alternative polyadenylation (10–12), splicing (13,14) and RNA turnover (15,16). In addition to these nuclear functions, PABPN1 has also been directly linked to the pioneer round of translation in the cytoplasm (17). More recently the role of PABPN1 has further expanded to include stimulation of RNA exosome-mediated turnover of non-coding RNAs including the long non-coding RNA (lncRNA) *NEAT1* (16) and the human telomerase RNA, *TERC* (14). Thus, PABPN1 plays a role in the production and maintenance of multiple classes of critical cellular RNAs.

*To whom correspondence should be addressed. Tel: +1 404 727 4546; Email: acorbe2@emory.edu
Correspondence may also be addressed to Grace K. Pavlath. Tel: +1 404 727 3590; Email: gpavlat@emory.edu

Consistent with broad requirements for PABPN1 in various steps critical to the production of mature RNAs, the PABPN1 protein is ubiquitously expressed (18); however, mutation of the *PABPN1 gene* causes muscle-specific pathology that manifests as OPMD (5). In fact, the most common mutation found in OPMD is a modest trinucleotide repeat expansion within the coding region of the *PABPN1* gene that expands an N-terminal alanine tract in PABPN1 from 10 alanines to 13 alanines (5). Furthermore, OPMD is primarily inherited in an autosomal dominant manner (19,20), which means that having just one copy of alanine-expanded PABPN1 is sufficient to cause pathology. While toxic aggregates of alanine-expanded PABPN1 have long been thought to be the underlying cause of disease (21–27), a growing number of studies have provided evidence that a more complex model of pathogenesis where loss of PABPN1 function, potentially through sequestration in aggregates could contribute to disease phenotypes (28,29).

Although numerous critical functions have now been ascribed to PABPN1, very little is known about the protein-binding partners that PABPN1 interacts with to perform these functions. Indeed, studies to identify PABPN1 interactors in muscle have not been performed. Past experiments that sought to define PABPN1 interactors employed yeast-two-hybrid screens with brain and human skeletal muscle cDNA libraries to identify the RNA binding proteins hnRNP A1, hnRNP A/B (25) and the transcriptional co-activator SKIP (30). Most other studies have used recombinant proteins or cell lines to investigate candidate-based interactions of PABPN1 with a variety of proteins (7,8,22,31). While valuable insight into PABPN1 function has been gained from these studies, it is critical to identify the proteins that interact with PABPN1 in muscle, the tissue most susceptible to expression of alanine-expanded PABPN1. The identification of novel protein interactions of PABPN1 in muscle could not only help to better define the critical functions of PABPN1 in muscle cells, but also provide insight into the pathways most susceptible to PABPN1 dysfunction in OPMD.

In this study, we utilize mass spectrometry to identify a number of PABPN1 interactors in mouse skeletal muscle including Matrin3 (MATR3). MATR3 was originally identified as a nuclear matrix protein containing both DNA and RNA binding domains (32,33) with a wide variety of functions ranging from DNA damage response to transcriptional and post-transcriptional regulation of cellular and viral RNAs (34–36). We demonstrate that MATR3 controls the post-transcriptional processing of shared transcripts with PABPN1 in muscle cells and is required for myogenesis. MATR3 and PABPN1 also bind and regulate the steady state levels of *Neat1* lncRNA, which is critical for paraspeckles (37–39), a nuclear subdomain previously linked to MATR3 (40). We provide evidence that both PABPN1 and MATR3 are required for proper paraspeckle physiology and function. We extend our analysis of paraspeckles to a mouse model that genocopies OPMD patients demonstrating altered paraspeckle physiology in the muscle of these mice (41). Finally, we show that human myoblasts deficient in PABPN1 show altered paraspeckle function, which suggests that this role of PABPN1 is conserved. Together these data identify novel binding partners of PABPN1 in muscle cells and provide evidence that PABPN1, like MATR3, is required for proper function of *Neat1* lncRNA as well as paraspeckle function.

MATERIALS AND METHODS

Cell culture

All cultured cells were maintained in a humidified incubator with 5% CO_2 at 37°C. Both murine and human primary myoblasts were cultured in growth media (Ham's F10, 20% FBS, 5 ng/ml bFGF, 100 U/ml penicillin G, 100 mg/ml streptomycin) on collagen-coated (Bovine Collagen I, Gibco) dishes. To induce differentiation, cells were plated on dishes coated with Entactin–Collagen IV–Laminin (ECL; Upstate Biotechnology) in growth media and shortly thereafter switched to differentiation media (DMEM, 1% Insulin–Transferrin–Selenium-A (ITS) supplement (Invitrogen), 100 U/ml penicillin G and 100 mg/ml streptomycin). C2C12 myoblasts (ATCC) were maintained in growth media (DMEM, 10% FBS, 100 U/ml penicillin G and 100 mg/ml streptomycin) and switched to DMEM supplemented with 1% horse serum and ITS supplement to induce differentiation. Both murine and human primary myoblast cultures were greater than 99% myogenic cells.

Animals

Wildtype C57BL/6 mice (The Jackson Laboratory, Bar Harbor, ME, USA) were used for most experiments. Some experiments utilize an OPMD mouse model with one allele of wildtype (Ala10) *PABPN1* replaced by mutant *PABPN1* that encodes the alanine-expanded (Ala17) PABPN1 variant that is present in OPMD patients (41). All experiments were performed in accordance with approved guidelines and ethical approval from Emory University's Institutional Animal Care and Use Committee and in compliance with the National Institutes of Health.

Blue native polyacrylamide gel electrophoresis (BN-PAGE)

BN-PAGE analysis was performed as per (42). Briefly, cells were lysed in native lysis buffer (10 mM HEPES, 150 mM NaCl, 0.5% NP-40) and protein concentration was determined using a BCA assay. Seventy-five micrograms of lysate was resolved on a 4–20% Criterion Biorad polyacrylamide gel under native conditions (anode buffer: 25 mM imidiazole, pH 7.5; cathode buffer: 50 mM tricine, 7.5 mM imidazole, 0.02% coomasie G250) for 3 h at 90 V. For immunoblotting proteins were transferred to PVDF membrane (50 mM tricine, 7.5 mM imidazole) at 20 V for 3 h. Native protein standards (Novex, Life technologies) were run on native gel to determine approximate sizes of the protein complexes being resolved.

Glycerol density gradients

Cells were lysed in native lysis buffer [10 mM HEPES pH 7.5, 2 mM $MgCl_2$, 10 mM KCl, 0.5% NP-40, 0.5 mM EDTA, 150 mM NaCl, 1 mM DTT and cOmplete Protease Inhibitor Cocktail (Sigma)]. 1.5 mg of cell lysate in 300 μl volume was layered on top of 10–30% glycerol gradients [10

mM HEPES pH 7.5, 2 mM $MgCl_2$, 10 mM KCl, 0.5 mM EDTA and 150 mM NaCl] in 14 × 89 mm tubes (Beckman Coulter), and spun in a SW41Ti rotor (Beckman Coulter) at 30 000 × RPM for 16 h at 4°C. Gradients were fractionated top to bottom into 500 μl fractions.

Immunoblotting

Cell lysates were prepared in Radioimmunopreciptation assay (RIPA) buffer supplemented with protease inhibitors (cOmplete protease inhibitor tablet (Sigma)). Protein concentrations were determined using a bicinchoninic acid (BCA) assay, and equal amounts of lysates were boiled in reducing sample buffer and resolved on 4–20% Criterion TGX polyacrylamide gels (Bio Rad). Proteins were transferred to nitrocellulose membranes and incubated for at least 1 h in blocking buffer (5% non-fat dry milk in TBS–Tween (0.1%)). This was followed by an overnight incubation at 4°C in primary antibody diluted in blocking buffer. Primary antibodies were detected using species specific HRP conjugated secondary antibodies followed by incubation with enhanced chemiluminescence substrate (ECL, Sigma). Chemiluminescence was detected by exposing blots to autoradiography film (Daigger). Primary antibodies used in this study are as follows: anti-PABPN1 (1:4000) (9,18,43), anti-PABPC1 (1:2500, Santa Cruz), anti-ARC (1:1000, RND Biosystems), anti-Histone H3 (1:5000, Abcam), anti-MATR3 (1:4000, Bethyl Labs), anti-GAPDH (1:1000, Bethyl Labs), anti-CPSF73 (1:1000, Abcam), anti-EXOSC10 (Bethyl Labs, 1:1000), anti-Myogenin (F5D, 1:100, Hybridoma bank), anti-Tubulin (1:4000, Sigma), anti-Flag (1:2500, M2, Sigma), anti-HSP90 (1:2000, Santa Cruz), anti-MAT2A (1:500, Bethyl Labs), anti-SFPQ (1:1000, Sigma), anti-His tag (1:500, Santa Cruz), anti-GST (1:1000, Santa Cruz), anti-TDP-43 (1:2000, Proteintech).

Two-dimensional polyacrylamide gel electrophoresis (2D-PAGE)

Lysates were resolved by BN-PAGE as described earlier, the gel lane to be resolved in a second dimension was excised as a whole and placed in an eppendorf tube. Reducing sample buffer was added to the tube and boiled for 2 min. The gel lane was placed in the well of a Mini-PROTEAN TGX™ 7 cm IPG/Prep protein gel and resolved by SDS-PAGE and immunoblotted.

Immunoprecipitations

Cultured cells or tissue were homogenized in IP buffer [50 mM HEPES, 125 mM NaCl, 5 mM EDTA, 0.5% NP-40, 1 mM DTT, cOmplete mini protease inhibitor cocktail (Sigma)]. Homogenate was sonicated on ice five times at 0.5% output for 10 s and then passed through a 27-gauge syringe five times. Cellular membranes and debris were removed by centrifugation at 13 000 rpm for 15 min. The supernatant containing soluble proteins was collected and protein concentration was determined using a bicinchoninic acid (BCA) assay. After removing 10% of lysate for input, PABPN1 antibody and control rabbit IgG for endogenous IPs or M2 Flag magnetic beads (Sigma) for IP from electroporated muscle were added to clarified cell lysates, followed by incubation on an end-over-end rotator at 4°C overnight. The next day for immunoprecipitating endogenous PABPN1, Protein G magnetic beads (Dynabeads; Invitrogen) were added to the lysate for 1 h end-over-end at room temperature. After the 1-h incubation, beads were magnetized and washed three times with cold IP buffer. The washed beads were either submitted for mass spectrometric analysis or used for immunoblotting. For immunoblotting protein complexes were eluted with reducing sample buffer [250 mM Tris–HCl, 500 mM DTT, 10% SDS, 0.5% bromophenol blue, 50% glycerol].

Liquid chromatography and tandem mass spectrometry

To identify PABPN1 interacting proteins, on-bead mass spectrometry was employed. Following wash steps, dynabeads from control and ZC3H14 immunoprecipitates were resuspended in 8 M urea, 100 mM NaHPO4, pH 8.5 (50 μl final volume) and treated with 1 mM dithiothreitol (DTT) at 25°C for 30 min, followed by 5 mM iodoacetimide (IAA) at 25°C for 30 min in the dark. The samples were then diluted to 1 M urea with 50 mM ammonium bicarbonate (final volume 400 μl) and digested with lysyl endopeptidase (Wako; 1.25 ng/μl final concentration) at 25°C for 4 h and further digested overnight with trypsin (Promega; 1.25 ng/μl final concentration) at 25°C. The resulting peptides were desalted with a Sep-Pak C18 column (Waters) and dried under vacuum. Each sample was resuspended in loading buffer (0.1% formic acid, 0.03% trifluoroacetic acid, 1% acetonitrile) and analyzed independently by reverse-phase liquid chromatography coupled with tandem mass spectrometry (LC–MS/MS) as essentially previously described with slight modification. Briefly, peptide mixtures were loaded onto a C18 nanoLC column (75 μm i.d., 15 cm long, 1.9 μm resin from Dr Maisch GmbH) and eluted over a 5–30% gradient (Buffer A: 0.1% formic acid; Buffer B: 0.1% formic acid in 100% AcN). Eluates were monitored in a MS survey scan followed by 10 data-dependent MS/MS scans on a Q-Exactive plus Orbitrap mass spectrometer (Thermo Scientific, San Jose, CA, USA). The acquired MS/MS spectra were searched against a concatenated target decoy mouse reference database (v.62) of the National Center for Biotechnology Information (downloaded 14 November 2013 with 30 267 target entries) using the SEQUEST Sorcerer algorithm (version 4.3.0, SAGE-N). Searching parameters included: fully tryptic restriction, parent ion mass tolerance (±50 ppm), up to two missed trypsin cleavages and dynamic modifications for oxidized Met (+15.9949 Da). The peptides were classified by charge state and first filtered by mass accuracy (10 ppm for high-resolution MS), and then dynamically by increasing XCorr and ΔCn values to reduce protein false discovery rate to <1%. If peptides were shared by multiple members of a protein family, the matched members were clustered into a single group in which each protein identified by a unique peptide represented a subgroup.

Muscle injury

Muscle injury was performed as per (44,45). Briefly, wild-type male C57BL/6 mice anesthetized by intraperitoneal in-

jection of 91 mg/kg ketamine and 9.1 mg/kg xylazine were injured by injection of 50 μl of 1.2% $BaCl_2$ in PBS using a Hamilton syringe and a 27 G needle from the origin to the insertion of the left gastrocnemius muscle, whereas the contralateral muscle served as a control. For analgesia, mice were injected subcutaneously with 0.1 mg/kg buprenorphine before and after muscle injury. Mice were euthanized 7 days following injury using a CO_2 chamber. Control and injured gastrocnemius muscles were collected and homogenized for immunoblotting or immunoprecipitation analysis. All experiments were performed in accordance with approved guidelines and ethical approval from Emory University's Institutional Animal Care and Use Committee and in compliance with the National Institutes of Health.

Plasmids

The coding sequence for MATR3 was PCR-amplified with primers listed in Supplementary Table S1 and cloned into the pcDNA3.1 mammalian expression vector by the Emory Integrated Genomics Core (EIGC).

Cell transfections

For all plasmid and siRNA transfections cells were cultured in media without any added antibiotics. Plasmid transfections were carried out using DNA-In CRISPR reagent (Amsbio) as per the manufacturers protocols. siRNA transfections were done using Lipofectamine 2000 (Invitrogen) and a final concentration of 80 nM of duplex Stealth siRNA specific for PABPN1 or MATR3 (Invitrogen). After an overnight incubation, media containing transfection complexes was replaced with fresh growth media. siRNA-mediated depletion was assessed after 42 h of transfection.

Immunofluorescence and microscopy

Cells were rinsed in PBS and fixed in 3.7% formaldehyde (v/v in PBS) for 15 min. Fixed cells were washed twice with PBS for 5 min each and permeabilized in 0.3% Triton-X 100 for 10 min. This was followed by incubation in blocking buffer (3% bovine serum albumin in PBS) for 1 h. To detect endogenous PABPN1 and transfected myc-tagged proteins, fixed cells were incubated overnight at 4°C with anti-PABPN1 (1:500), anti-MATR3 (1:1000, Bethyl labs) or anti-myc (1:500, Cell Signaling) antibodies followed by staining with Texas Red or fluorescein-conjugated secondary antibodies (Jackson Labs). Position of the nucleus was marked by incubation with Hoechst 33342 (ThermoFisher Scientific) or DAPI (Sigma). Fluorescent or Phase images were acquired using a microscope (Axiovert 200 M; Carl Zeiss MicroImaging, Inc.) with a 0.3 NA 10× (Cellular Proliferation Assay), 20× (Phase images for differentiation), 60× (*Neat1* FISH) or 100× (SFPQ staining) Plan-Neofluar objective (Carl Zeiss MicroImaging, Inc.) and camera (QImaging) with OpenLab 5.5.0 software (Improvision).

Recombinant protein expression

Plasmids encoding GST only, GST-MATR3, His-PABPN1 were transformed into BL21 (DE3) *Escherichia coli* cells. Single colonies were inoculated into 2-ml cultures and grown overnight to saturation. These starter cultures were used to inoculate 50 ml of media. Cultures were grown at 37°C until they reached an $A_{600\,nm}$ of 0.4–0.6. Protein expression was induced with 200 μM isopropyl β-D-1-thiogalactopyranoside for 5 h at 30°C. Following protein induction, cells were pelleted and frozen at −80°C. Frozen cell pellets were resuspended in lysis buffer [20 mM Tris–HCl, pH 8.0, 100 mM NaCl, 5% glycerol, 4 μM 2-mercaptoethanol, 1 mM phenylmethylsulfonyl fluoride] and lysed by sonication. GST-tagged proteins and His-tagged PABPN1 were purified on Glutathione Sepharose 4B (GE Healthcare) or Ni-NTA agarose (Qiagen) respectively according to the manufacturer's directions.

GST binding assays

For GST-MATR3 binding to His-PABPN1, GST only or GST-MATR3 were immobilized on Glutathione Sepharose 4B (GE Healthcare) and incubated with purified soluble His-PABPN1 in 1 ml IPP100 buffer [10 mM Tris–HCl, pH 8, 100 mM NaCl, 0.1% NP-40] supplemented with 10 mg/ml BSA, 2 mM DTT, and protease inhibitor mixture (0.2 mM phenylmethylsulfonyl fluoride, 3 ng/ml pepstatin A, leupeptin, aprotinin, and chymostatin) for 2 h at 4C with mixing. Beads were washed three times with IPP100 buffer and boiled in reducing sample buffer [250 mM Tris–HCl, 500 mM DTT, 10% SDS, 0.5% bromophenol blue, 50% glycerol], followed by immunoblotting for GST and PABPN1.

Crosslinking and immunoprecipitation of RNA (CLIP)

UV-crosslinking and immunoprecipitation of RNA was performed using standard methods (46). Briefly, myoblasts grown in 100 mm collagen coated dishes, rinsed twice with ice-cold PBS, crosslinked with UV (254 nm) and lysed with an equal pellet volume of RIPA-2 buffer [50 mM Tris, pH 7.4, 150 mM NaCl, 0.1% SDS, 1% Triton X-100, 1% Na-deoxycholate, 1 mM EDTA, RNase OUT (Invitrogen), and 1 cOmplete protease inhibitor tablet (Sigma)]. Protein A-Dynabeads (Invitrogen) were incubated with either rabbit IgG or MATR3 antibody (Bethyl Labs). Beads coated in antibody were resuspended in NT2 buffer [50 mM Tris–HCl, pH 7.4, 150 mM NaCl, 1 mM $MgCl_2$, 0.05% Nonidet P-40] supplemented with RNase OUT (Invitrogen) and 1 mM DTT. Thawed and clarified cell lysates were added, and the bead/antibody/cell lysate mixture was incubated at 4°C overnight while tumbling end-over-end. After incubation, beads were magnetized and washed five times with cold NT2 buffer. RNA was released from bound proteins by Proteinase K treatment and input and bound RNA was isolated with TRIzol (Invitrogen) according to the manufacturer's instructions.

RNA Isolation and reverse transcription

Total RNA was isolated using TRIzol reagent (Invitrogen) as per the manufacturer's instructions. cDNA was synthesized by reverse transcription reactions using Moloney murine leukemia virus reverse transcriptase (Invitrogen)

with random hexamers as per the manufacturer's instructions. One microgram of RNA was used per reverse transcription reaction, and 10 ng of cDNA was used per well for quantitative real time PCR.

Quantitative real-time PCR

For qRT-PCR analyses, 1 μg of total RNA was transcribed to cDNA as described above. Relative mRNA levels were measured by quantitative PCR analysis of triplicate samples of 10 ng of cDNA with QuantiTect SYBR Green Master Mix using an Applied Biosystems real time machine (ABI). Fold change was calculated using the ΔΔCt method, by normalizing to the HPRT transcript for the first ΔCt and to either control IgG IP samples (siRNA mediated knockdown followed by endogenous protein RNA-immunoprecipitation) or primers sets for the coding sequence (siRNA mediated knockdown affect on polyadenylation site usage and retained intron) for the second ΔCt. Statistical significance was determined using Student's *t*-test. A list of primers used for these analyses is shown in Supplemental Table S1.

Cellular proliferation assay

Cell proliferation of primary myoblasts was measured using the ClickIt EdU Alexa Fluor 594 Imaging Kit (Molecular Probes) as per the manufacturer's protocol. Briefly, cells were labeled with 10 μM EdU for 3 h followed by detection with an azide linked Alexa Fluor dye. DNA was marked with Hoechst 33342 and images were obtained using a 10× objective as described earlier. Images were analyzed using the CellProfiler software to determine the number of EdU positive nuclei under the various siRNA treatments. The CellProfiler software was programmed to identify individual Hoechst signals as nuclei, and to identify and measure the intensity of any overlapping red (Alexa Fluor 594) signal as EdU positive nuclei. The integrated signal intensities of Alexa Fluor 594 signal from all images were exported to Microsoft Excel and used to generate a frequency table for each siRNA treatment.

Bulk poly (A) tail length assay

Bulk poly (A) tails were analyzed as described previously (9). In brief, T4 RNA ligase was used to 3′-end label total RNA (5–10 μg) with [^{32}P]-pCp (cytidine 3′,5′-bisphosphate) (Perkin Elmer), followed by digestion with RNase A and T1. Digested RNA were resolved on TBE-Urea (90 mM Tris-borate, 2 mM EDTA, 8 M urea) 7% polyacrylamide gels, dried using a Bio-Rad gel dryer and exposed to a phosphorscreen. Gel images were obtained using a Typhoon phosphorimager and quantified using ImageQuant software.

RNA stability assay

Cells were treated with 5 μg/ml Actinomycin D to inhibit transcription and lysed after 30 min, 1 h, 2 h and 4 h of treatment. RNA was isolated and reverse transcribed as described previously. Transcript levels were assessed using qRT-PCR by normalizing to *Gapdh* and the 30 min time point.

S-adenosylmethionine measurement

SAM measurements were carried out using the BridgeIt®S-Adenosyl Methionine (SAM) Fluorescence Assay Kit as per manufacturers protocol 42 h after siRNA-mediated depletion of PABPN1 or MATR3. Fluorescence measurements were obtained using a Biotek Plate Reader.

Cellular fractionation

Cells were scraped and centrifuged at 1000 × g for 5 min in cold PBS. Cell pellets were resuspended in 200 μl of lysis buffer [10 mM Tris at pH 8.0, 140 mM NaCl, 1.5 mM $MgCl_2$, 0.5% Igepal, 2 mM vanadyl ribonucleoside complex (VRC)] and incubated for 5 min on ice. Twenty microliters of lysate was removed for total RNA and the rest of the lysate was centrifuged at 1000 × g for 3 min at 4°C to pellet the nuclei. The supernatant was collected as cytoplasm and cleared by centrifugation at 13 000 rpm for 10 min at 4°C. The nuclear pellet was washed twice and resuspended in 200 μl of lysis buffer.

RNA editing analysis

Taq DNA polymerase was used to perform PCR using primers specific for amplifying an edited region of the *Ctn* 3′ UTR from cDNA. PCR products were gel purified, cloned into TOPO-TA vector and transformed into DH5α chemically competent bacteria. Agar plates with positive transformants were sent for colony sequencing (MCLAB Sequencing) with a universal M13 primer. Sequences were aligned to unedited genomic sequence and edited sites were identified as A to G conversions.

CRISPR Cas9 knockout

Primary human myoblasts were transfected in six-well plates with plasmids from Horizon Discovery that encode both a guide RNA expressed from a *U6* promoter and a Cas9 endonuclease expressed under a hCMV IE1 promoter. Transfected myoblasts were diluted in 10 cm collagen coated plates to allow for clonal selection. Selected clones were expanded and assessed for knockout of *PABPN1* using qRT-PCR and immunoblot analysis.

Fluorescent *in situ* hybridization

RNA-FISH was performed using a Stellaris RNA-FISH probe (Mouse Neat1_5 Quasar® 570 Dye) as per the manufacturers protocol. Briefly, cells were washed twice with PBS and fixed in 3.7% formaldehyde for 15 min. Fixed cells were washed with PBS followed by overnight permeabilization at 4°C in 70% ethanol. Permeabilized cells were incubated overnight at 37°C in hybridization buffer containing FISH probe (125 nM). Cells were washed and incubated with DAPI to mark the nucleus, followed by mounting in Vectashield® Mounting Medium.

RESULTS

PABPN1 exists in multiple protein complexes

Critical to defining the role of PABPN1 in muscle is the identification of proteins that interact with PABPN1 in

muscle cells. We performed a majority of our experiments in primary myoblasts, which are myogenic precursor cells that can be isolated from murine skeletal muscles and maintained in cell culture (9,47). These myoblasts when differentiated into multinucleated myotubes represent a widely accepted model of *in vitro* myogenesis that provides an ideal model system amenable to the study of muscle physiology (9).

As a first step to identifying PABPN1 interacting proteins, we analyzed whether PABPN1 exists in protein complexes in primary myotubes. Total cell lysates obtained from control primary myotubes and myotubes overexpressing PABPN1 (PABPN1 O/E) were analyzed by blue native polyacrylamide gel electrophoresis (BN-PAGE). PABPN1 overexpression was employed to ensure that the higher molecular weight bands observed were specific to PABPN1. SDS-PAGE followed by immunoblot analysis with a PABPN1 antibody was performed to confirm the overexpression of PABPN1 in the PABPN1 O/E myotubes (Figure 1A, bottom). Blue native gels blotted and probed with a PABPN1 antibody (9) reveal that PABPN1 is detected in multiple bands (indicated by arrowheads in Figure 1A, top), ranging from ∼66 kilodaltons (kDa) up to several megadaltons (MDa) in size. The higher molecular weight bands increase in intensity in the lane with lysate from PABPN1 O/E myotubes, confirming that these bands are indeed specific to PABPN1 (Figure 1A). To ensure that the complexes detected with BN-PAGE contain PABPN1, we performed a follow-up 2D PAGE analysis (Figure 1B). The lane containing lysate from PABPN1 O/E myotubes was resolved by BN-PAGE, excised as a whole and resolved in a second dimension by SDS-PAGE. Immunoblot analysis confirmed the presence of PABPN1 in the multiple bands detected in the blue native gel (arrowheads in Figure 1B). Thus, PABPN1 exists in multiple protein complexes in primary myotubes.

To further examine PABPN1 protein complexes, we analyzed sedimentation of PABPN1 in glycerol density gradients. Total cell lysate from primary myoblasts or primary myotubes was loaded and spun on 10–30% glycerol gradients (Figure 1C). Immunoblot analysis of fractions collected from the density gradients shows that PABPN1 migrates in multiple fractions of the gradient and shifts to heavier fractions in lysates from myotubes as compared to lysates from proliferating myoblasts (boxed in Figure 1C). Fractions from the glycerol gradients were also resolved by BN-PAGE and immunoblotted to detect PABPN1 (Figure 1D). The heavier fractions (13–21) from myotubes show slower migrating bands (boxed in black) that are not present in lysates obtained from myoblasts. These results imply that PABPN1 exists in protein complexes in muscle cells that change in composition over the course of differentiation from myoblast to myotube.

Protein interactions of PABPN1 in skeletal muscle

To identify proteins that interact with PABPN1 in skeletal muscle, the ideal experiment would be to immunoprecipitate endogenous PABPN1 from muscle together with associated proteins. However, PABPN1 (Figure 2A) and other RNA binding proteins (Supplementary Figure S1) are present at low levels in skeletal muscles (18,48) as compared to other tissues, which makes this approach challenging. To circumvent the challenge of low PABPN1 expression, we utilized a well-characterized transgenic mouse (A10.1) that overexpresses PABPN1 only in skeletal muscles under the control of a skeletal muscle actin promoter (23). We confirmed the increase in PABPN1 levels in lysates prepared from skeletal muscle from these mice (Figure 2B), and then performed immunoprecipitations from these skeletal muscle lysates with control rabbit IgG or PABPN1 antibody (9) followed by mass spectrometric analysis of co-immunoprecipitating proteins (Figure 2C). Detection of two or more peptides in the PABPN1 antibody immunoprecipitation and no peptides detected in the control IgG immunoprecipitation was used as a cutoff for the identification of PABPN1 interacting proteins (Figure 2D). Although expression of most nuclear RNA binding proteins is indeed low in skeletal muscles, we identified peptides corresponding to PABPN1 as well as two additional poly (A) binding proteins (PABPC1 and PABPC4). We also identified hnRNP proteins (HNRNPQ and HNRNPC) consistent with previous findings from yeast two hybrid experiments (25).

In addition to the poly (A) binding proteins and hnRNPs, we identified the DNA/RNA binding proteins, Pur-alpha (PURA) (49) and Matrin3 (MATR3) (32,33), as well as Apoptosis repressor with caspase-recruitment domain protein (ARC) (50) as novel PABPN1 interacting proteins (listed in Figure 2D). We confirmed two of the protein interactions identified by mass spectrometry by demonstrating that the polyadenosine RNA binding protein PABPC1 and the anti-apoptotic protein ARC co-immunoprecipitate with PABPN1 from skeletal muscle lysate obtained from the transgenic mouse model overexpressing PABPN1 (Figure 2E). These results define proteins that interact with PABPN1 in skeletal muscle under these experimental conditions.

MATRIN3 interacts with PABPN1 in muscle

The protein Matrin3 (MATR3) identified in our mass spectrometry results (Listed in Figure 2D) as a potential binding partner for PABPN1 is a nuclear matrix protein associated with multiple steps of RNA processing that is altered in vocal cord and distal myopathy as well as amyotrophic lateral sclerosis (51,52). To determine whether PABPN1 and MATR3 interact in skeletal muscles lysate, we immunoprecipitated PABPN1 from regenerating muscles six days after barium chloride-mediated injury. This experimental condition was selected because regenerating skeletal muscle provide an environment with active mRNA metabolism and increased levels of expression of RNA binding proteins (18). Immunoblot analysis of the immunoprecipitated fractions shows that MATR3 is enriched specifically in the PABPN1 immunoprecipitation from skeletal muscle lysates with no significant enrichment with control IgG (Figure 3A). To further validate the interaction between PABPN1 and MATR3, we performed a reciprocal co-immunoprecipitation with an antibody to MATR3 (Supplementary Figure S2). The reciprocal immunoprecipitation demonstrates that MATR3 can immunoprecipitate PABPN1 from muscle cell lysate. As a positive control,

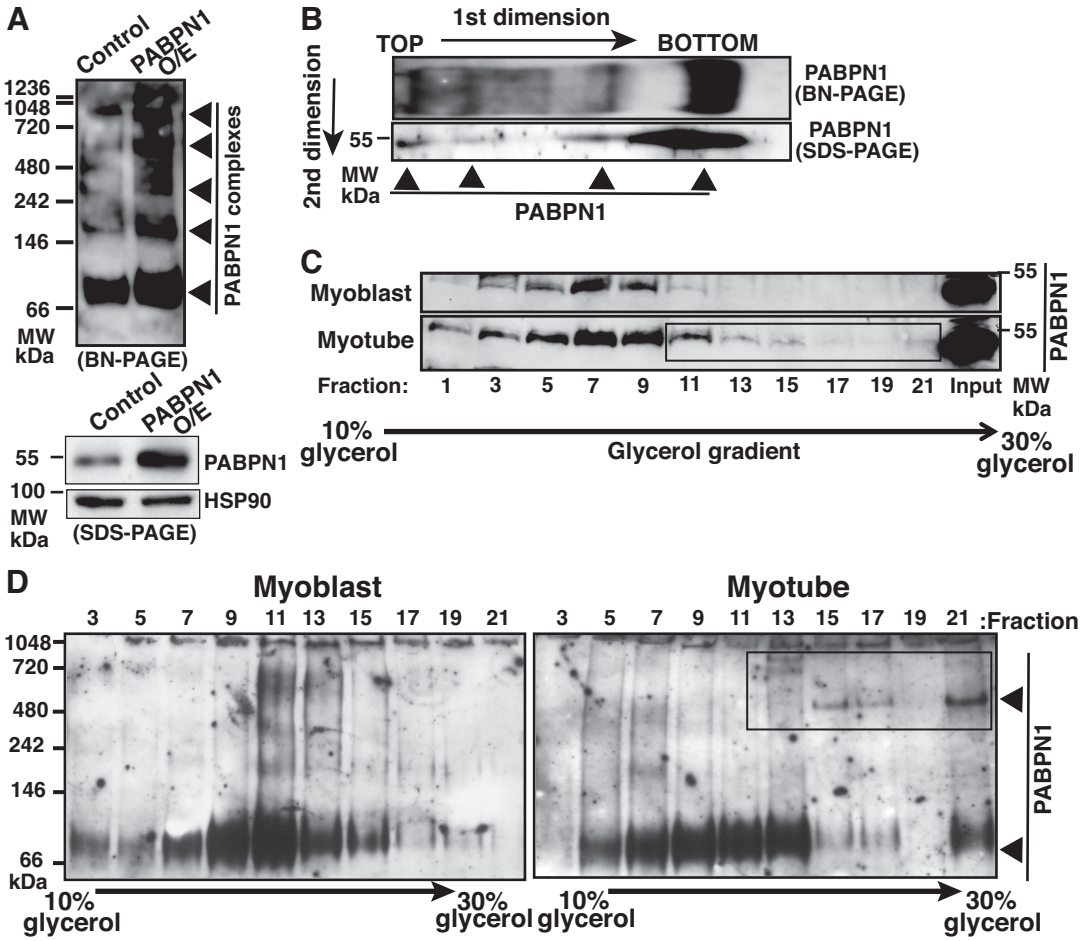

Figure 1. PABPN1 is present in multiple protein complexes. (**A**) Whole cell lysate from control myotubes or myotubes overexpressing PABPN1 (PABPN1 O/E) were resolved by blue native polyacrylamide gel electrophoresis (BN-PAGE) (top) and SDS-PAGE (bottom) and analyzed by immunoblotting with anti-PABPN1 antibody (9). Higher molecular weight bands potentially representing PABPN1 protein complexes are indicated by arrowheads. HSP90 SERVES as a loading control. (**B**) Whole cell lysate from myotubes overexpressing PABPN1 was resolved by BN-PAGE in the first dimension followed by SDS-PAGE in the second dimension. Immunoblotting was performed with anti-PABPN1 antibody to confirm the presence of PABPN1 in higher molecular weight bands (indicated by arrowheads). (**C**) Whole cell lysates from myoblasts (top) and myotubes (bottom) were analyzed by sedimentation through 10–30% glycerol gradients. Alternate gradient fractions from top to bottom were loaded and resolved by SDS-PAGE. Input was also loaded as a control. The presence of PABPN1 in the glycerol gradient fractions was detected by immunoblotting with an anti-PABPN1 antibody. The migration of PABPN1 in heavier fractions in lysates from myotubes is indicated by the box. (**D**) Whole cell lysate from primary myoblasts and differentiated myotubes were analyzed by sedimentation through 10–30% glycerol gradients. Alternate gradient fractions from top to bottom were loaded from left to right and resolved by Blue Native-PAGE (the sample representing fraction 19 was lost due to a technical issue). Immunoblotting with a PABPN1 antibody detects PABPN1 in a major band of ∼66 kDa and some fainter higher bands in fractions collected from myoblasts. PABPN1 appears in a band of higher molecular weight (∼480 kDa) in the heavier glycerol gradient fractions collected from myotubes (boxed in black).

we confirmed that both PABPN1 and MATR3 also co-immunoprecipitate PABPC1, which was identified previously as a protein interacting with MATR3 (53) and in this study as a PABPN1 interacting protein (Figure 2E).

As further confirmation that PABPN1 interacts with MATR3, PABPN1 was immunoprecipitated from a C2C12 mouse muscle cell line lysate prepared at various stages of differentiation (Supplementary Figure S3). Similar to regenerating muscles, differentiating muscle cells provide an environment of active gene expression and RNA processing (54,55). MATR3 co-immunoprecipitates with PABPN1 from C2C12 muscle lysate, with the interaction being most pronounced in lysates prepared from cells at Day 5 of differentiation. PABPN1 also co-immunoprecipitates with MATR3 from whole mouse brain lysate (Supplementary Figure S4) suggesting that this interaction is relevant in the context of another tissue with high levels of post-transcriptional RNA processing (56,57). As a positive control we confirmed that PABPN1 co-immunoprecipitates TDP43 from brain lysates, which was recently identified as a novel PABPN1 protein interactor in neuronal cells (58,59).

As a complement to immunoprecipitation experiments, we analyzed the intracellular localization of PABPN1 and MATR3 in muscle cells (Figure 3B). To simultaneously detect PABPN1 and MATR3, we transfected primary myoblasts with a plasmid expressing myc-tagged MATR3, which allows us to use a mouse monoclonal antibody against the myc tag to detect MATR3 and a rabbit polyclonal antibody to detect endogenous PABPN1. Immunocytochemistry shows the co-localization of endogenous

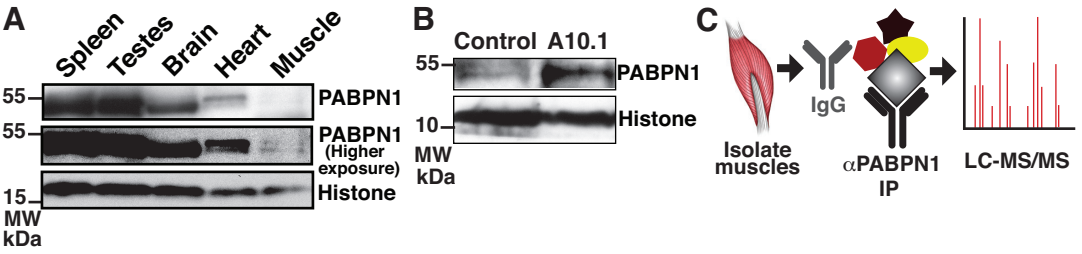

D PABPN1 interacting proteins

PABPC1	polyadenylate-binding protein 1
PABPC4	polyadenylate-binding protein 4 isoform 1
MATR3	matrin-3
ARC	nucleolar protein 3
HNRPQ	heterogeneous nuclear ribonucleoprotein Q
PURA	transcriptional activator protein Pur-alpha
HNRPC	heterogeneous nuclear ribonucleoproteins C1/C2

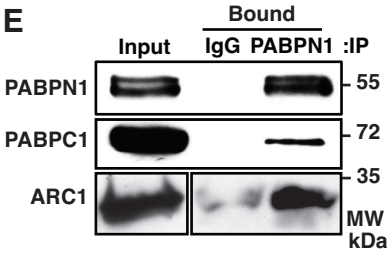

Figure 2. PABPN1 interacts with multiple proteins in skeletal muscle lysate. (**A**) Lysates collected from the indicated tissues were resolved by SDS-PAGE and analyzed by immunoblotting for PABPN1. Histone H3 serves as a loading control. A higher exposure of the PABPN1 immunoblot is shown to visualize PABPN1 in the skeletal muscle lysate. (**B**) Lysates obtained from control gastrocnemius skeletal muscle and gastrocnemius skeletal muscle transgenically overexpressing PABPN1 (A10.1) were resolved by SDS-PAGE and analyzed by immunoblotting for PABPN1. Histone H3 acts as a loading control. (**C**) A schematic outlining the experimental approach to identify PABPN1-interacting proteins in mouse muscle is shown. We isolate gastrocnemius muscles and then immunoprecipitate with either a PABPN1 antibody (9) or control IgG, followed by mass spectrometry as described in Material and Methods. (**D**) Table listing the PABPN1-interacting proteins that co-immunoprecipitate with PABPN1 from murine skeletal muscles is shown. (**E**) Protein interactions identified by mass spectrometry (PABPC1 and ARC1) were validated by co-immunoprecipitation from murine skeletal muscle lysates. The bound fractions from control (IgG) and PABPN1 immunoprecipitations (IP) were resolved by SDS-PAGE and immunoblotted for PABPN1, PABPC1 and ARC1. The Input is shown as a control. Results shown are typical of three independent experiments.

PABPN1 with myc-tagged MATR3 in discrete nuclear foci (Figure 3B), providing further evidence that these RNA binding proteins interact.

To further examine the interaction of PABPN1 with MATR3, we analyzed lysates prepared from C2C12 myotubes using glycerol density gradients. As shown in Figure 3C, MATR3 sediments in some of the same fractions as PABPN1, which could suggest that these proteins are present in a protein complex (boxed in black in Figure 3C). We also analyzed the fractions obtained from these glycerol density gradients for the migration pattern of protein components of the RNA-exosome (EXOSC10) and the cleavage and polyadenylation complex (CPSF73), both of which have been functionally associated with PABPN1 (8,15,16). Both EXOSC10 and CPSF73 show some overlap with PABPN1 that is distinct from the pattern observed with MATR3. In addition to being present in the same fractions in a density gradient, 2D-PAGE analysis shows that MATR3 is present in the same higher molecular weight bands as PABPN1 in lysates prepared from primary myotubes (Figure 3D). These data suggest that PABPN1 and MATR3 interact in protein complexes in muscle cells.

Given that PABPN1 and MATR3 are both RNA binding proteins (7,8,53), we assessed whether the interaction detected is RNA-dependent. Flag-tagged PABPN1 was expressed and immunoprecipitated from transfected primary myoblast lysates with or without RNase treatment (Figure 3E) and the immunoprecipitate was probed for MATR3. RNase treatment did not abolish the interaction of PABPN1 with MATR3, suggesting that this interaction is not RNA dependent (Figure 3E). To test for a direct interaction between PABPN1 and MATR3, we performed an *in vitro* binding assay with recombinant His-PABPN1 and GST-MATR3 (Figure 3F). His-PABPN1 was incubated with either control GST or GST-MATR3 protein followed by capture of GST proteins with Protein A Sepharose beads and immunoblotting for bound His-PABPN1. The specific enrichment of His-PABPN1 with GST-MATR3 but not with the control GST protein supports a direct interaction between PABPN1 and MATR3. Together these data show that MATR3 is a novel interacting partner of PABPN1 in cultured muscle cells and in skeletal muscle.

MATR3 is critical for *in vitro* myogenesis

Given that MATR3 interacts with PABPN1 in muscle and *MATR3* is mutated in a distal myopathy (51), we explored whether MATR3, like PABPN1 (9) binds to myogenic transcripts critical for myogenesis. We employed UV crosslinking coupled with RNA-immunoprecipitation (ClIP) to examine the interaction of MATR3 with both coding and non-coding RNAs. Results of this analysis using primary myoblasts (Figure 4) show that MATR3 binds to a number of key myogenic transcripts including both coding (Figure 4A) and non-coding RNAs (Figure 4B). These transcripts are critical for cellular function with some playing key roles in myogenesis (60–63).

Having demonstrated that MATR3 binds critical myogenic transcripts, we investigated whether MATR3 is important for myogenesis. Primary myoblasts were transfected with control siRNA or siRNA targeting either PABPN1 or MATR3. Immunoblotting was performed to confirm efficient depletion of PABPN1 and MATR3 in the cells transfected with siRNA (Figure 5A). Muscle cell function can

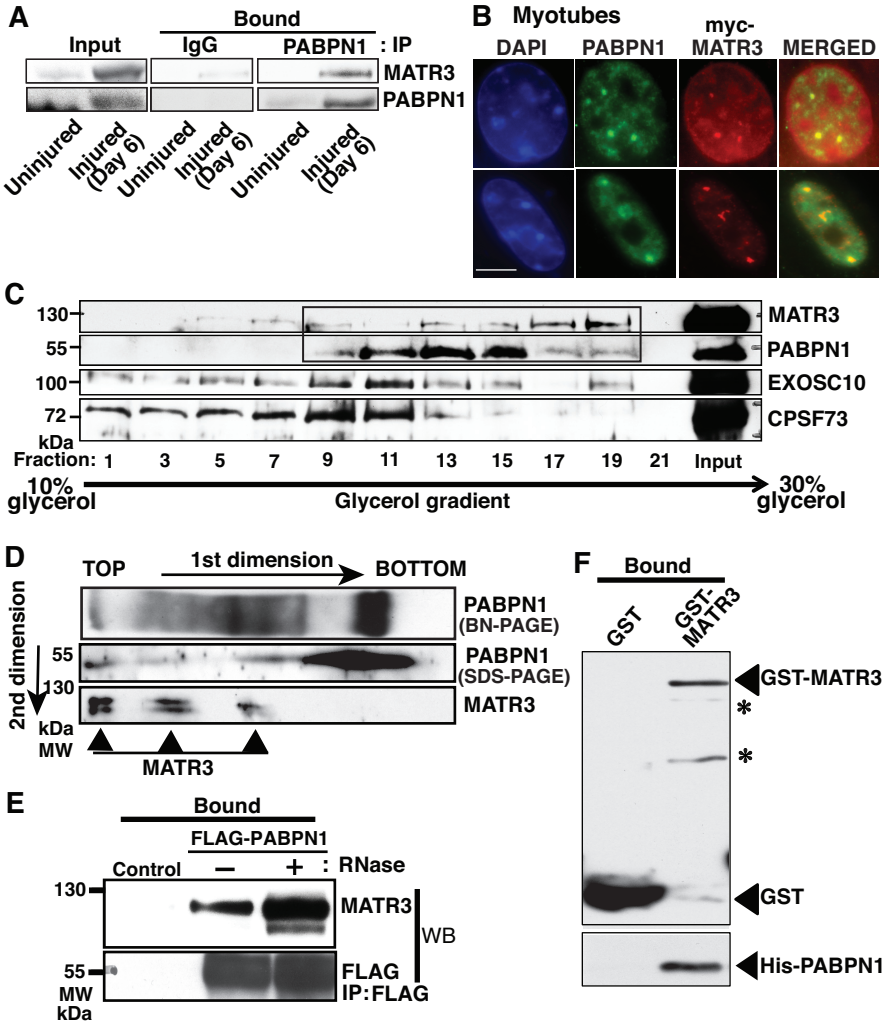

Figure 3. PABPN1 interacts with MATR3. (**A**) Input and bound samples from control (IgG) and PABPN1 immunoprecipitations (IP) from lysates obtained from uninjured muscles or injured muscles 6 days post-injury were resolved by SDS-PAGE and immunoblotted for PABPN1 and MATR3. Results shown are typical of three independent experiments. (**B**) Primary myoblasts were transfected with a plasmid expressing myc-MATR3 and differentiated into myotubes for 48 h. These transfected myotubes were stained with anti-PABPN1 antibody to detect endogenous PABPN1 (FITC/Green) and anti-myc antibody to detect myc-MATR3 (Texas red). Merged images of FITC and Texas red staining are shown to visualize co-localization (Yellow) in myonuclei. DAPI staining marks the nucleus. Four independent experiments were conducted with similar results. Representative images are shown for two independent myonuclei from independent transfections. (**C**) Lysates from C2C12 cell line myotubes were analyzed by sedimentation through 10–30% glycerol gradients. Gradient fractions from top to bottom were loaded from left to right and resolved by SDS-PAGE. An Input sample is shown on the right. Immunoblotting was performed to detect PABPN1 and MATR3 in the glycerol gradient fractions. The black box indicates fractions that contain both PABPN1 and MATR3. Immunoblotting was also performed to detect EXOSC10 (RNA exosome complex) and CPSF73 (cleavage and polyadenylation complex) in the fractions. (**D**) Whole cell lysate from primary myotubes was resolved by BN-PAGE in the first dimension followed by SDS-PAGE in the second dimension. Immunoblotting was performed to detect MATR3 and PABPN1 (indicated by arrowheads) in the same higher molecular weight bands. (**E**) Lysates from control primary myoblasts or primary myoblasts transfected with a plasmid expressing Flag-PABPN1 were either treated with RNase A (+) or left untreated (–), followed by immunoprecipitation with an anti-Flag antibody. Immunoblotting was performed to detect MATR3 and PABPN1. (**F**) Direct protein-protein interaction between MATR3 and PABPN1 was assessed by incubating recombinant His-PABPN1 with control GST protein alone or GST-MATR3, followed by a GST-pulldown and immunoblotting for GST and His-PABPN1. Asterisks indicate the positions of two degradation products of GST-MATR3.

be gauged by both the proliferative capacity of myoblasts and the ability of myoblasts to efficiently proceed through *in vitro* myogenesis, by differentiating and then fusing with one another to form multinucleated myotubes (9). To assess proliferation, myoblasts were labeled with a thymidine nucleoside analog, 5′-ethynyl-2′-deoxyuridine (EdU) that is incorporated into newly synthesized DNA. As is evident from the decrease in EdU staining, myoblasts depleted of PABPN1 or MATR3 show less proliferation when compared to myoblasts transfected with control siRNA (Figure 5B and C). To evaluate differentiation, primary myoblasts depleted of PABPN1 or MATR3 were plated at equal density and differentiated. Effects on differentiation were investigated by measuring the level of an early biochemical marker of differentiation, myogenin, 24 h after initiating differentiation (9,64) (Figure 5D). As compared to myoblasts transfected with control siRNA, cells depleted of MATR3 or PABPN1 show reduced levels of myogenin after 24 h of differentia-

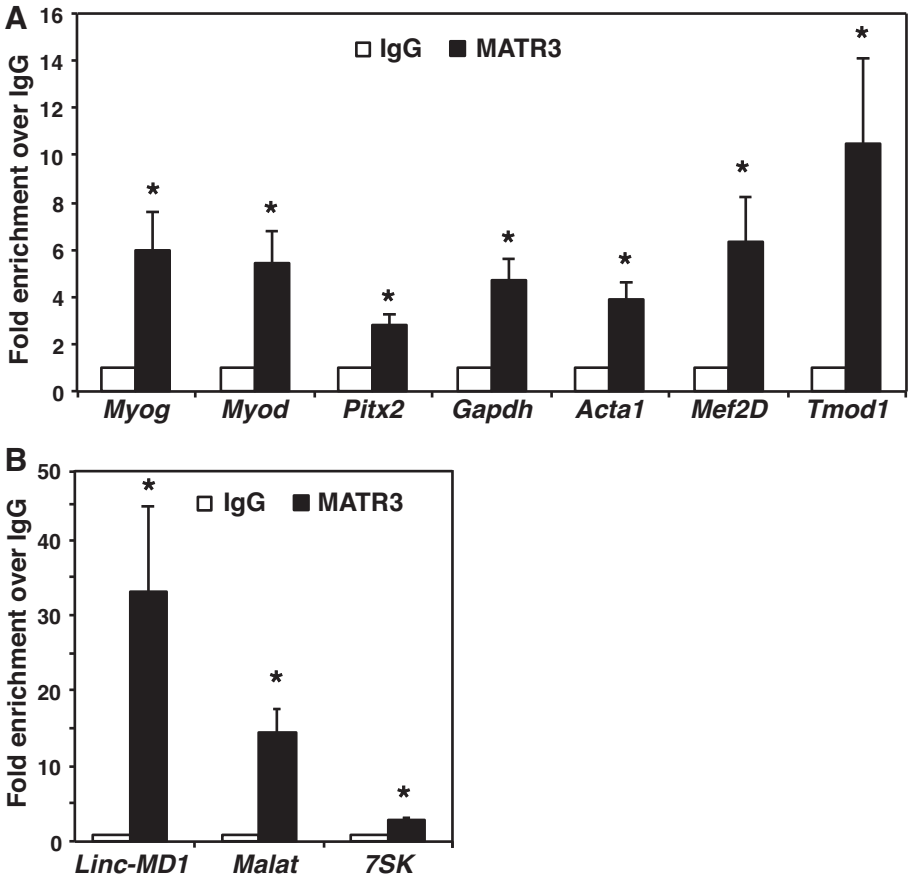

Figure 4. MATR3 binds to both coding and non-coding myogenic transcripts. To test for transcripts associated with MATR3, immunoprecipitations were performed from UV crosslinked primary myoblasts using control IgG antibody or MATR3 antibody. Bound RNAs, both (**A**) coding (*Myog, MyoD, Pitx2, Gapdh, Acta1, Mef2d and Tmod1*) and (**B**) non-coding (*Linc-MD1, Malat1 and 7SK*), were detected by qRT-PCR. For each transcript analyzed, the bound RNA was normalized to input and graphed as fold enrichment over binding to control IgG antibody, which was set to 1.0. Results are the average of three biological replicates. Error bars represent standard error of the mean (*$P < 0.05$).

tion. Differentiation in control myoblasts or myoblasts depleted of MATR3 or PABPN1 was also analyzed by visually monitoring myoblast fusion and myotube formation using phase-contrast microscopy. Myoblasts depleted of MATR3 show fewer and smaller mature multinucleated myotubes compared to control myoblasts after 48 h of differentiation, although this defect is not as severe as that observed upon PABPN1 depletion (Figure 5E). These results from an *in vitro* model of myogenesis suggest that much like PABPN1, MATR3 binds coding and non-coding transcripts and is critical for normal cellular proliferation and differentiation.

Regulation of shared transcripts by MATR3 and PABPN1

Given that the best-characterized role of PABPN1 is in the regulation of poly (A) tail length (7–9), we assessed whether MATR3 regulates bulk poly (A) tail length. This experiment that uses an established assay that examines 3′ end-labeled poly (A) tracts (9), shows that myoblasts depleted of MATR3 do not show a significant change in bulk poly (A) tails as compared to myoblasts transfected with control siRNA (Figure 6A and B). In contrast myoblasts depleted of PABPN1 show shorter bulk poly (A) tails as previously reported (Figure 6A and B) (9). These data suggest that regulation of bulk poly (A) tail length likely does not account for the requirement of MATR3 for efficient *in vitro* myogenesis.

As the depletion of MATR3 does not affect bulk poly (A) tail length, we explored whether MATR3 could impact any of the other RNA processing functions ascribed to PABPN1. In addition to a well-characterized role in control of poly (A) tail length (7,9), PABPN1 plays critical roles in polyadenylation site (PAS) selection (10–12), poly (A) polymerase-mediated decay of transcripts (65) and turnover of long non-coding RNAs (lncRNAs) (16). To determine if MATR3 also regulates these facets of RNA metabolism, we examined candidate RNAs in myoblasts depleted of either PABPN1 or MATR3. We first examined 3′ UTR length, which depends on the selection of either a proximal or distal polyadenylation site (66,67). As depicted in the schematic (Figure 7A), changes in polyadenylation site selection can be analyzed with quantitative real time PCR using primers designed to detect either total transcript levels (total) or to specifically detect the longer 3′ UTR (distal) that results from the selection of the distal PAS (PAS2) (Figure 7A). We assessed the PAS usage of candidate transcripts that have either previously been identified as PABPN1 targets (*Tmod1,*

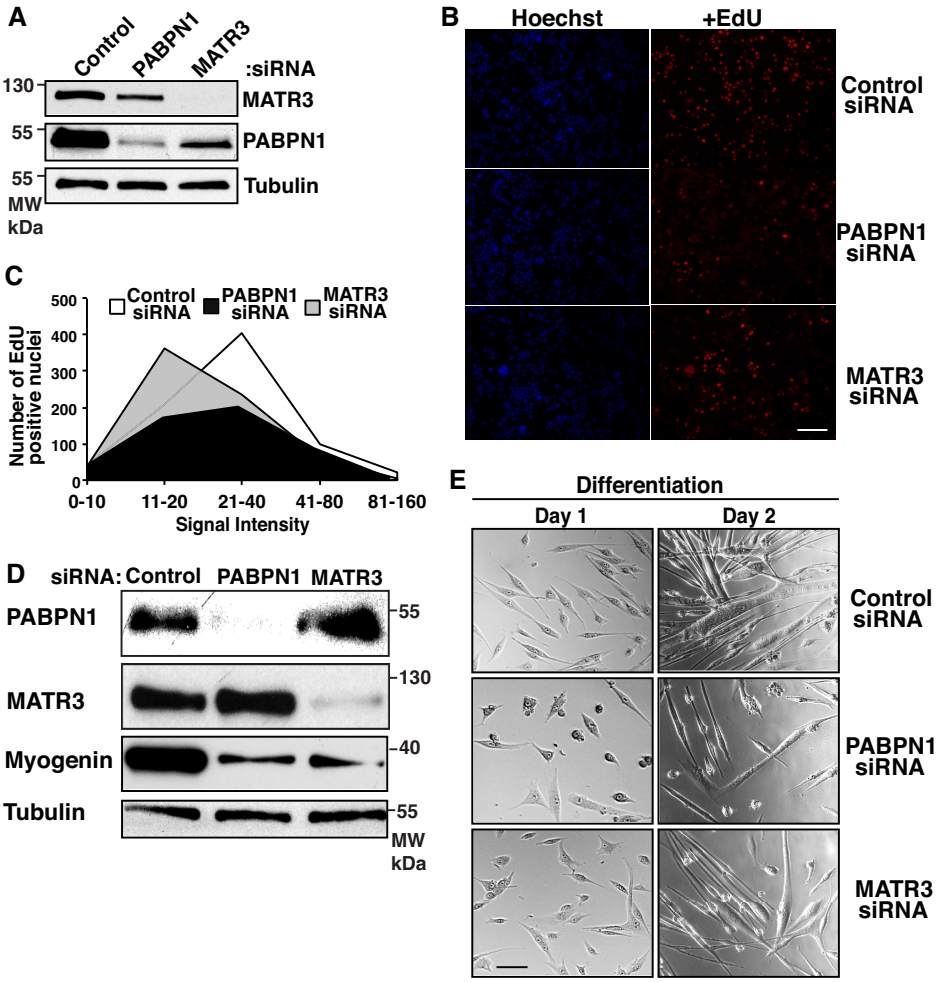

Figure 5. MATR3 is required for normal myoblast proliferation and differentiation. (**A**) Primary myoblasts were transfected with Control siRNA or siRNA targeting either PABPN1 or MATR3. Immunoblotting was performed with anti-PABPN1 and anti-MATR3 antibodies to confirm depletion of PABPN1 and MATR3, respectively. Tubulin serves as a loading control. (**B**) Cells were labeled with EdU and actively proliferating cells were detected by staining with an anti-Edu Alexa Fluor 594 antibody. Hoechst was used to mark the position of the nuclei. (**C**) The number of EdU positive nuclei and Alexa Fluor 594 signal intensity was quantified using Cell Profiler software. A frequency graph was generated by plotting signal intensity of Edu staining on the X-axis and the number of Edu positive primary myoblasts binned on the Y-axis. (**D**) Primary myoblasts transfected with Control siRNA or siRNA targeting PABPN1 or MATR3 were differentiated. Protein extracts obtained from primary myotubes were analyzed by immunoblotting for PABPN1, MATR3 and Myogenin. Tubulin serves as a loading control. (**E**) Phase-contrast microscopy images were captured to monitor *in vitro* myogenesis. Representative images are shown from Day 1 and Day 2 of differentiation for cells transfected with Control siRNA or siRNA targeting PABPN1 or MATR3.

Psme3 or *Vldlr*) (11) or are regulated by a change in PAS usage during myogenesis (*Timp2*) (55). Depletion of MATR3 results in significantly decreased use of the distal PAS of *Tmod1*, which is an effect opposite to the increase we detect in distal PAS usage that results upon depletion of PABPN1 in primary myoblasts (Figure 7B and Supplementary Figure S5). No statistically significant change in PAS usage was observed for the other transcripts tested. This result suggests that while both PABPN1 and MATR3 can regulate polyadenylation site selection, they can have differential effects on 3′ UTR length.

Recent studies have defined a role for PABPN1 in poly (A) polymerase-mediated decay of transcripts containing retained introns (65). Transcripts containing these retained introns are hyperadenylated by poly (A) polymerase, which is stimulated by PABPN1. These hyperadenylated transcripts are then degraded by the nuclear RNA exosome. Consistent with a key role for PABPN1 in this process, depletion of PABPN1 causes an increase in the steady-state level of transcripts containing these retained introns. To explore a potential role for MATR3 in modulating the levels of transcripts with intron retention, we assessed the levels of the *Mat2a* transcript containing the retained intron. *Mat2a* encodes s-adenosylmethionine synthase, which catalyzes the formation of s-adenosylmethionine, a methyl group donor for a wide variety of biological reactions (68). We employed quantitative real time PCR using primers designed to detect either the total transcript or specifically detect the transcript containing the retained intron. Knockdown of either PABPN1 or MATR3 causes a significant accumulation of the *Mat2a* transcript containing the retained intron (Figure 7C and Supplementary Figure S5). Concomitant with the increased levels of retained intron-containing *Mat2a* transcript, we detect a decrease in MAT2A protein

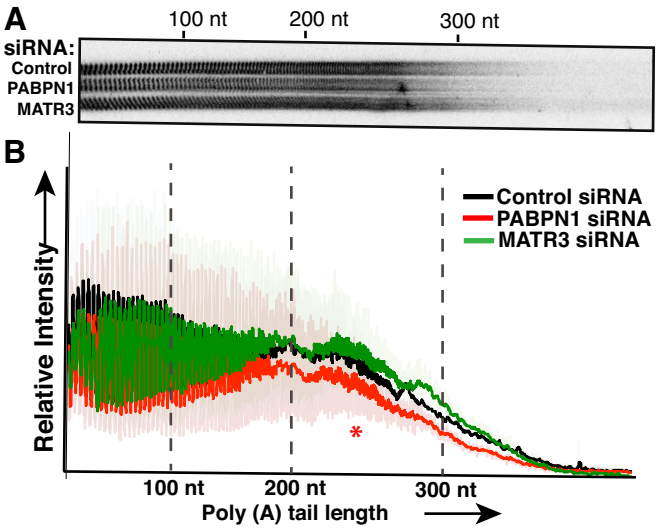

Figure 6. MATR3 does not regulate bulk polyadenylation in primary myoblasts. (**A**) Total RNA isolated from myoblasts transfected with Control siRNA or siRNA targeting PABPN1 or MATR3 was analyzed for bulk poly (A) tail length by resolving 3′-end labeled poly(A) tracts on a denaturing polyacrylamide gel as described in Materials and Methods. (**B**) Bulk poly (A) tail lengths were quantified using ImageQuant software. Relative intensities of the bulk poly (A) tails on the Y-axis were plotted against increasing poly (A) tail lengths on the X-axis. Approximate size of RNA size markers are indicated by dotted lines.

levels (Figure 7D) and a corresponding decrease in levels of s-adenosyl methionine (SAM) in myoblasts depleted of PABPN1 or MATR3 as compared to control myoblasts (Figure 7E). Cumulatively, these data suggest that PABPN1 and MATR3 can regulate post-transcriptional RNA processing of the same transcripts in myoblasts, and that their effect on RNA processing can be concordant or discordant depending on the regulatory process or candidate transcript analyzed.

Loss of PABPN1 or MATR3 function alters paraspeckle physiology

Our analysis of mRNA processing in primary myoblasts demonstrated shared roles for MATR3 and PABPN1 in RNA processing. As both PABPN1 and MATR3 have also been implicated in the processing of non-coding RNAs (16,53), we extended our analysis to assess whether MATR3 regulates *Neat1*, a long non-coding RNA that is regulated by PABPN1 (16). Myoblasts depleted of either MATR3 or PABPN1 show significantly increased levels of *Neat1* RNA (Figure 8A) when compared to control myoblasts. RNA immunoprecipitation with an anti-MATR3 antibody confirms that, like PABPN1, MATR3 binds *Neat1* RNA in primary myoblasts (Figure 8B). The increase in steady-state levels of *Neat1* RNA can be attributed to an increase in the stability of the *Neat1* transcripts as determined by analyzing the decay of *Neat1* after treatment of primary myoblasts with the transcriptional inhibitor, Actinomycin D (Supplementary Figure S6), which aligns with the previously characterized role of PABPN1 in exosome-mediated lncRNA decay (16).

Given the regulation of *Neat1* RNA by both PABPN1 and MATR3 and the essential role of *Neat1* in paraspeckle formation and maintenance (37–39), we assessed the effects of depleting either PABPN1 or MATR3 on paraspeckle physiology in muscle cells. Primary myoblasts transfected with control siRNA or siRNA directed against PABPN1 or MATR3 were fixed and probed for *Neat1* RNA by fluorescent *in situ* hydridization (FISH). As shown in Figure 8C and quantified in Figure 8D, myoblasts depleted of PABPN1 or MATR3 show an increase in the number of *Neat1* RNA foci when compared to control myoblasts, which suggests that PABPN1 and MATR3 regulate paraspeckle morphology.

Paraspeckles are the site of adenosine to inosine (A to I) editing for numerous cellular RNAs (40,69). One such RNA, *Ctn*, is regulated by multiple editing events in its 3′ UTR that cause nuclear retention in paraspeckles (69). We quantified A to I editing of *Ctn* RNA to determine if the increase in *Neat1* levels and paraspeckle number observed in myoblasts depleted of PABPN1 or MATR3 corresponds to altered *Ctn* A to I editing (Figure 8E). RNA obtained from control myoblasts or myoblasts depleted of PABPN1 or MATR3 was reverse transcribed to obtain complementary DNA, followed by PCR amplification, cloning and sequencing of an edited region of the 3′ UTR of *Ctn* (Figure 8E). Sequencing of multiple clones from independent knockdowns of PABPN1 or MATR3 in muscle cells reveals a marked increase in the levels of editing of *Ctn* RNA when compared to control cells (Figure 8F, Supplementary Figure S7). To ensure that the increase in A to I editing is dependent on the increased levels of *Neat1* RNA, cells depleted of PABPN1 or MATR3 were co-transfected with siRNA targeting *Neat1*. qRT-PCR was performed to confirm efficient depletion of *Neat1* (Supplementary Figure S8). Sequencing analysis of the *Ctn* 3′ UTR in cells deficient for PABPN1 or MATR3 but also depleted of *Neat1* reveals a return towards control levels of editing when compared to cells only deficient in PABPN1 or MATR3 (Figure 8F, Supplementary 7), confirming that altered editing is dependent on the levels of *Neat1* transcript.

To further analyze paraspeckles, we assessed the distribution of the paraspeckle protein SFPQ in myoblasts depleted of PABPN1 or MATR3 using glycerol density gradients. SFPQ is present in fractions 3–5 in control myoblasts but shifts toward lighter fractions (fractions 1–3) in lysates from myoblasts with reduced levels of PABPN1 (Figure 8G). The distribution of SFPQ is also changed in lysates obtained from myoblasts depleted of MATR3, with a markedly increased amount of SFPQ present in the lightest fraction (fractions 1) (Figure 8G). This shift in the distribution of SFPQ in density gradients suggests a change in normal paraspeckle composition. Immunofluorescence microscopy was employed to assess the distribution of SFPQ in muscle cells deficient for PABPN1 or MATR3 compared to control myoblasts (Supplementary Figure S9A). As with the results obtained by analyzing *Neat1* via FISH, SFPQ staining reveals an increase in paraspeckle number. We verified that the foci identified by SFPQ immunofluorescence correspond to paraspeckles by treating cells with a low concentration of the transcriptional inhibitor Actinomycin D, which causes a relocation of paraspeckle proteins to per-

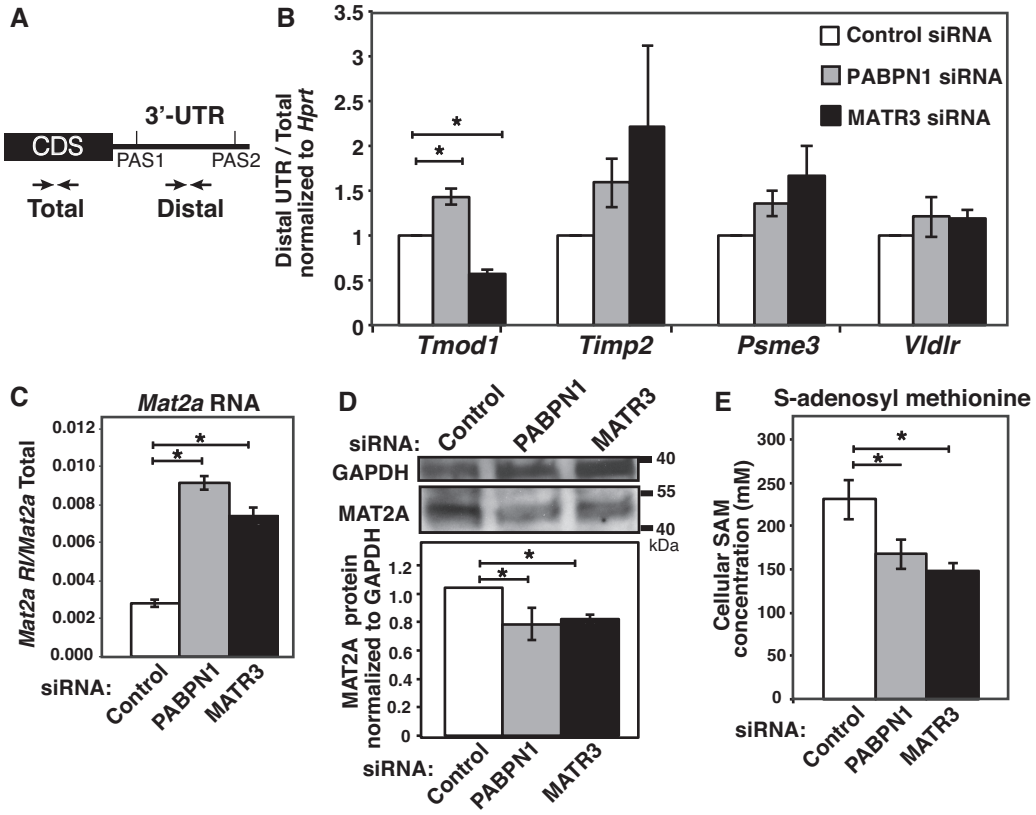

Figure 7. Regulation of shared transcripts by MATR3 and PABPN1. (**A**) Schematic of qRT-PCR strategy with primers specific to the coding sequence (CDS) used to detect Total transcript or the distal 3′ UTR to analyze differential use of the proximal polyadenylation site (PAS1) or the distal polyadenylation site (PAS2) in candidate mRNAs. (**B**) Primary myoblasts were transfected with control siRNA or siRNA targeting PABPN1 or MATR3. qRT-PCR with primers detecting the CDS (Total) and the long 3′ UTR (distal UTR) was utilized to quantify levels of *Tmod1, Timp2, Psme3* and *Vldlr* RNAs. The levels of the longer 3′ UTR (distal 3′ UTR) are presented relative to the Total mRNA (Total) normalized to *Hprt*. The experiment was carried out at least five independent times. Error bars represent standard error of the mean (*$P < 0.05$). (**C**) qRT-PCR was performed to assess the levels of *Mat2a* transcript containing the retained intron (*Mat2a-RI*) and total *Mat2a* transcript in myoblasts depleted of PABPN1 and MATR3 as compared to control myoblasts. The levels of the *Mat2a* transcript containing the retained intron (*Mat2a-RI*) are presented relative to the total mRNA (*Mat2a*-Total) normalized to *Hprt*. The experiment was carried out seven independent times. Error bars represent standard error of the mean (*$P < 0.05$). (**D**) MAT2A protein levels were assessed in primary myoblasts transfected with Control siRNA or siRNA targeting either PABPN1 or MATR3. Immunoblotting was performed using a MAT2A antibody with GAPDH serving as a loading control. Levels of MAT2A were quantified by densitometry using Fiji imaging software and are presented as fold change relative to samples from control siRNA normalized to GAPDH. The experiment was carried out three independent times. Error bars represent standard error of the mean (*$P < 0.05$). (**E**) Levels of S-adenosyl methionine (SAM) were measured in control primary myoblasts and primary myoblasts depleted of PABPN1 or MATR3 as described in Materials and Methods. The experiment was carried out three independent times. Error bars represent standard error of the mean (*$P < 0.05$).

inucleolar caps (70,71) (Supplementary Figure S9B). Taken together these data indicate that MATR3 and PABPN1 regulate *Neat1* and contribute to normal paraspeckle physiology and function.

Given the alteration of paraspeckle physiology in primary myoblasts deficient for PABPN1, we assessed whether this defect is present *in vivo* in muscles of a mouse model of OPMD that genocopies the *PABPN1* patient mutation (41). This model carries one copy of alanine-expanded *PABPN1* (Ala17) and one copy of wildtype *PABPN1* (Ala10) as compared to control mice that have two wildtype copies of *PABPN1* (Ala10/Ala10). In contrast to earlier OPMD disease models that rely on overexpression of alanine-expanded PABPN1 (23), this model of OPMD expresses alanine-expanded PABPN1 at endogenous levels and shows molecular and mitochondrial defects associated with muscle degeneration (41). Muscle cells lysates prepared from this OPMD mouse model (Ala10/Ala17) were resolved on density glycerol gradient and compared to muscle lysate from wildtype control (Ala10/Ala10). SFPQ immunoblots performed on fractions obtained from these glycerol gradients show that the distribution of SFPQ *in vivo* is shifted to lighter fractions (fractions 1–3) in muscle lysate prepared from OPMD muscle when compared to wildtype muscle (fractions 5 and 6) (boxed in Figure 8H).

Regulation of paraspeckles by PABPN1 is conserved in human myoblasts

To extend this analysis to primary human muscle cells, we generated CRISPR-CAS9 mediated PABPN1-knockout human myoblasts (PABPN1-KO). Immunofluorescent staining (Figure 9A) and immunoblots (Figure 9B) using a PABPN1 antibody were performed to confirm efficient depletion of PABPN1. Paraspeckles play a critical role in the nuclear retention of a well-characterized subset of

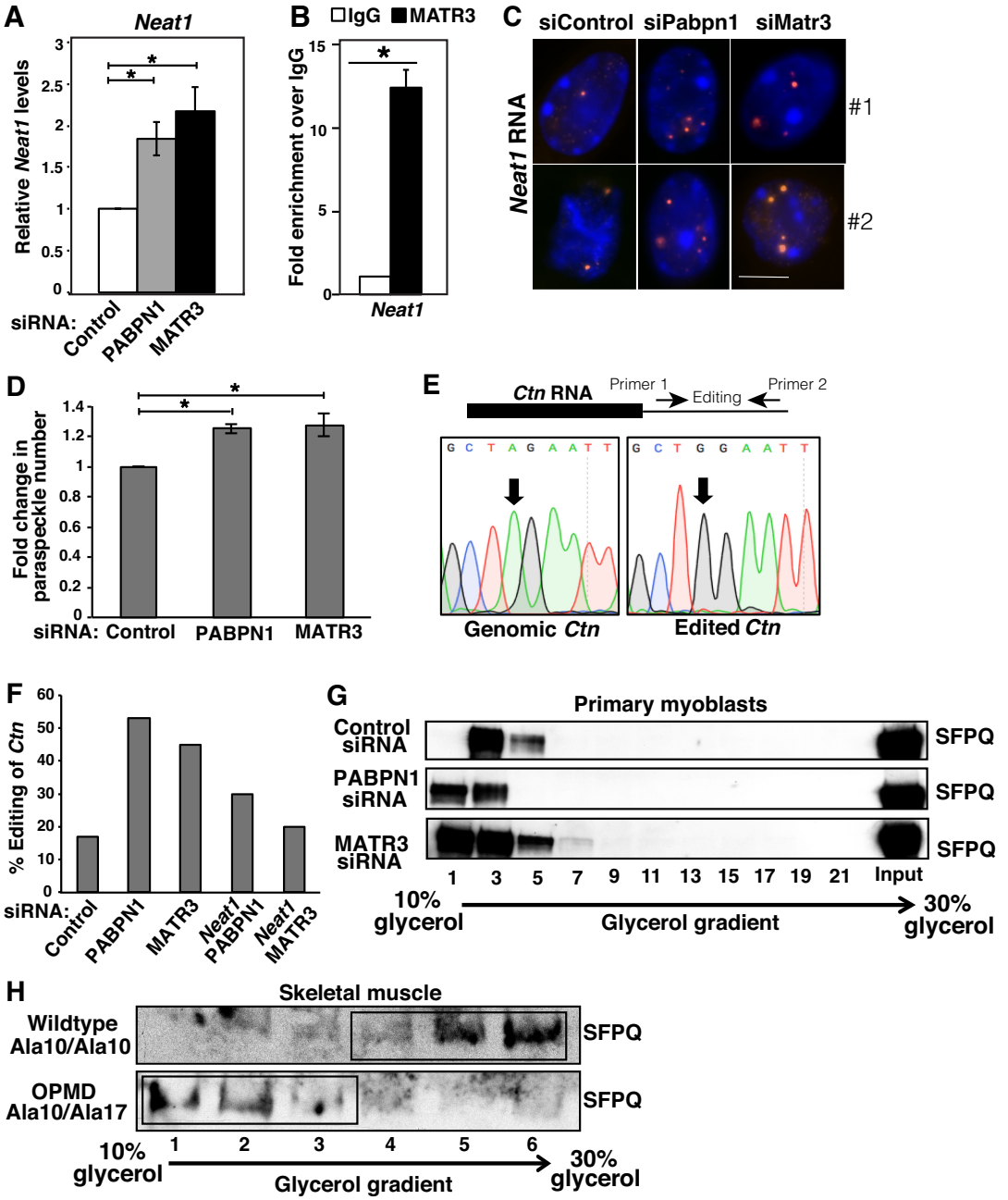

Figure 8. PABPN1 and MATR3 regulate nuclear paraspeckle function. (**A**) Primary myoblasts were transfected with Control siRNA or siRNA targeting PABPN1 or MATR3. qRT-PCR was performed to assess the levels of *Neat1* lncRNA. Levels of *Neat1* RNA are presented as fold change relative to the control transcript, *Gapdh* and normalized to Control siRNA. (**B**) RNA immunoprecipitations were performed from primary myoblasts using control IgG or MATR3 antibody. Bound RNA is normalized to input and is presented as fold enrichment over binding to control IgG antibody, which was set to 1.0. Results are representative of three independent experiments. Error bars represent standard error of the mean (*$P < 0.05$). (**C**) *Neat1* RNA-FISH was performed using a Cy3 labeled *Neat1* probe, to visualize paraspeckles in control myoblasts or myoblasts depleted of PABPN1 or MATR3. Two independent myonuclei are shown. DAPI staining marks the nucleus. (**D**) Paraspeckles were counted in at least 100 cells from independent fields for each siRNA (Control, PABPN1, MATR3) and graphed as fold-change relative to control siRNA treatment. Experiments were carried out three independent times. Error bars represent standard error of the mean (*$P < 0.05$). (**E**) A diagram representing the PCR amplification of an edited section of the *Ctn* 3′ UTR (69) to analyze adenosine to inosine (A to I) RNA editing. Also shown is a typical electropherogram detecting an RNA editing event (arrow) that is identified as an adenosine (A) to guanosine (G) change in the sequenced PCR product. (**F**) PCR products amplified from cDNA were cloned and sequenced. The number of sequenced A to I editing events in control myoblasts, myoblasts depleted of PABPN1 or MATR3 and myoblasts with a concomitant depletion of *Neat1* RNA (*Neat1*+PABPN1 and *Neat1*+MATR3) is presented as the percentage of sequenced clones with at least one RNA editing event (% Editing of *Ctn*). (**G**) Whole cell lysates prepared from primary myoblasts transfected with control siRNA or siRNA targeting PABPN1 or MATR3 were analyzed by sedimentation through 10–30% glycerol gradients. Gradient fractions from top to bottom were loaded left to right together with an 'Input' lane and resolved by SDS-PAGE, followed by immunoblotting for the paraspeckle component SFPQ. (**H**) Skeletal muscle lysate obtained from wildtype mice (Ala10/Ala10) or mice carrying one wildtype and one mutant allele (Ala10/Ala17) of *PABPN1* was analyzed by sedimentation through 10–30% glycerol gradients. Glycerol gradient fractions 1 to 6 (top to bottom) were loaded left to right and resolved by SDS-PAGE followed by immunoblotting for SFPQ.

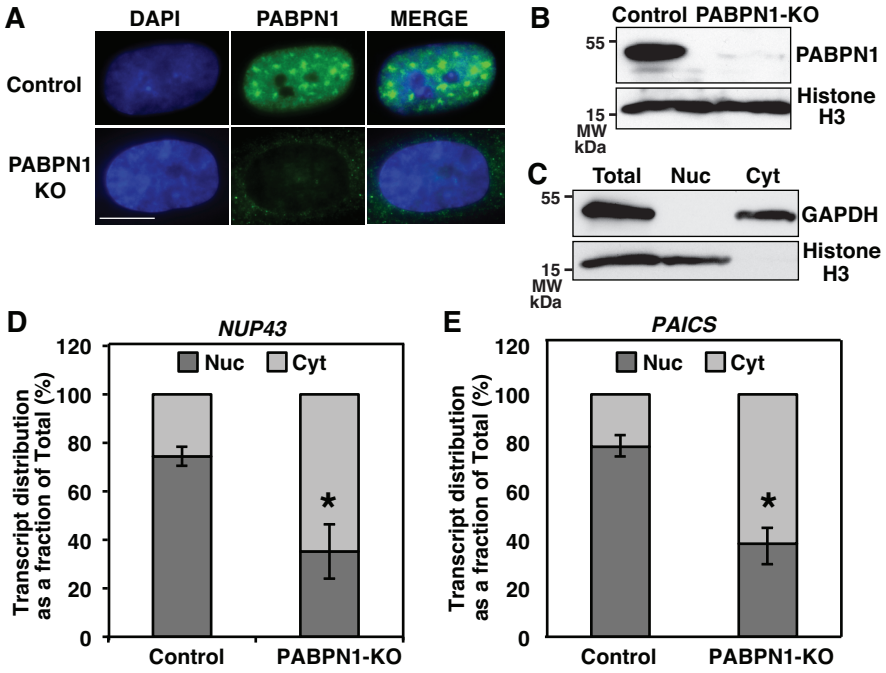

Figure 9. The requirement for PABPN1 in paraspeckle function is conserved in human myoblasts. (**A**) Immunofluorescence was performed to detect PABPN1 protein in control human myoblasts and PABPN1-KO human myoblasts created with CRISPR-Cas9 as described in Materials and Methods. DAPI staining marks the position of the nucleus. (**B**) Immunoblot analysis was performed to analyze levels of PABPN1 protein in PABPN1-KO human myoblasts as compared to control human myoblasts. Histone H3 serves as a loading control. (**C**) Myoblasts were fractionated to determine nuclear-cytoplasmic localization of candidate transcripts. Efficient nucleocytoplasmic fractionation was confirmed by immunoblotting with Histone H3 and GAPDH antibodies to mark the nuclear (Nuc) and cytoplasmic (Cyt) fractions, respectively. (**D**) The steady-state distribution of known paraspeckle-mediated nuclear retained transcripts (*NUP43* and *PAICS*) was established by performing qRT-PCR using transcript specific primers on the nuclear (Nuc) and cytoplasmic (Cyt) fractions prepared from control and PABPN1-KO human myoblasts. *NUP43* and *PAICS* transcripts were normalized to the endogenous transcript *RPLP0* and are presented here as a percentage of total transcript Transcript distribution as a fraction of total). Experiments were performed four independent times. Error bars represent standard error of the mean (*$P < 0.05$).

transcripts (*NUP43, PAICS*) in human cells (72,73). To assess whether loss of PABPN1 affects the localization of these transcripts, nuclear and cytoplasmic fractions were prepared from control human myoblasts and PABPN1-KO myoblasts. We verified efficient fractionation of human myoblasts by immunoblotting for GAPDH and Histone H3 as cytoplasmic and nuclear markers, respectively (Figure 9C). We employed qRT-PCR to analyze the level of *NUP43* (Figure 9D) and *PAICS* (Figure 9E) transcript in the nuclear and cytoplasmic fractions. Both the *NUP43* and *PAICS* transcripts are significantly shifted to the cytoplasm in human myoblasts deficient for PABPN1 as compared to wildtype human myoblasts. The mislocalization of these transcripts suggests, that much like in murine cells, normal paraspeckle function is disrupted in human myoblasts deficient for PABPN1.

DISCUSSION

In this study, we employed an unbiased mass spectrometry approach to identify proteins that interact with PABPN1 in skeletal muscle. Among several PABPN1 interacting proteins identified, we characterized Matrin3 (MATR3) and provide evidence for shared functions of MATR3 and PABPN1 in RNA processing in muscle cells. Both MATR3 and PABPN1 can regulate alternative polyadenylation and contribute to the turnover of transcripts containing retained introns. Furthermore, MATR3 and PABPN1 control normal paraspeckle physiology and function by regulating the lncRNA *Neat1*. We also find that depletion of PABPN1 or MATR3 disrupts paraspeckle physiology in primary myoblasts. This disruption of paraspeckles is recapitulated by the expression of endogenous levels of alanine-expanded PABPN1 in muscles of an OPMD mouse model. Finally, based on analysis of CRISPR-Cas9 edited cells, we show that the requirement for PABPN1 to support proper paraspeckle function is likely conserved in human myoblasts. This work provides the first unbiased identification of PABPN1-interacting partners in skeletal muscle, examines the role of MATR3, and defines a shared role for PABPN1 together with MATR3 in paraspeckle maintenance.

The PABPN1 interacting proteins identified in this study included the polyadenosine RNA binding proteins, PABPC1 and PABPC4. Both PABPC1 and PABPC4 are primarily cytoplasmic proteins (74) that can shuttle into the nucleus, particularly under conditions of cellular stress (75,76). While PABPC1 has well characterized cytoplasmic roles in modulating translation and mRNA stability (77,78), past experiments have provided evidence suggesting a nuclear role wherein PABPC1 can bind poly (A) tails of pre-mRNA simultaneously with PABPN1 (79). The lesser-characterized PABPC4 binds A-rich sequences in the 3′ UTR of candidate transcripts and is critical for ery-

throid differentiation (80). Compensatory nuclear relocalization of PABPC4 has been reported in cell lines depleted of PABPN1 (81), which suggests that PABPC4 could regulate some of the same steps of RNA processing as PABPN1. Together with the poly (A) binding proteins, PABPN1 also co-immunoprecipitated the heterogeneous ribonucleoproteins C and Q (hnRNP C and Q). These hnRNPs are associated with various aspects of RNA processing including splicing (82–84), mRNA stability (85) and translational control (86,87). Using a yeast two-hybrid approach, other hnRNPs (hnRNP A1 and hnRNP A/B) were previously identified as PABPN1-interactors (25). Immunohistochemical analysis of OPMD patient muscle sections showed that hnRNP A1 could be sequestered with PABPN1 in insoluble nuclear aggregates (25), potentially preventing hnRNP A1 from performing its normal function in muscle. In fact, a recent study reported that alanine-expanded PABPN1 causes mislocalization of the splicing factor, SC35, from nuclear speckles, causing splicing defects in OPMD (88). Consistent with these findings, sequestration of hnRNP C and Q in nuclear aggregates in OPMD muscle could contribute to the molecular pathology of OPMD. This loss of function by sequestration in aggregates could also apply to other identified protein-binding partners of PABPN1.

The apoptosis repressor with caspase recruitment domain (ARC) also co-purifies with PABPN1. ARC is highly expressed in heart and skeletal muscle (50) and is a potent inhibitor of apoptosis (89,90). An *ARC* constitutive knockout mouse model shows skeletal muscle abnormalities and dysfunction associated with increased apoptotic signaling and mitochondrial defects (91). PABPN1 has been reported to have an anti-apoptotic function (29,92), with overexpression of wildtype PABPN1 providing protection from apoptotic stimuli and from the deleterious effects of alanine-expanded PABPN1 in both cellular and mouse models of OPMD (29). Thus, the interaction between PABPN1 and ARC could contribute to this anti-apoptotic function of PABPN1. Future work will be required to test whether the interaction between PABPN1 and ARC is critical for skeletal muscle homeostasis.

Two other proteins identified as PABPN1 interacting partners are DNA/RNA binding proteins, Pur-alpha and Matrin3. Pur-alpha (PURA), is a single stranded DNA and RNA binding protein (49,93) implicated in multiple cellular processes ranging from transcription to RNA transport and translation (94,95). PURA interacts and aggregates with defective FUS protein that is causative of amyotrophic lateral sclerosis (ALS) (96). MATR3 was originally identified as a nuclear matrix protein with DNA and RNA binding domains (32,33). Critical roles for MATR3 have been reported in DNA damage repair (34), alternative splicing (97), RNA stability (53) and nuclear retention of hyperedited RNAs (40). The interaction between MATR3 and PABPN1 was conserved in brain as well as skeletal muscle (Supplementary Figure S4), which suggests that this could be a more general interaction relevant in multiple cell types and tissues. However, the disruption in protein-protein interaction between MATR3 and mutant Lamin A contributes to the pathogenesis of laminopathies that manifest as myopathies (98). Additionally, mutations in the *MATR3* gene are linked to a distal myopathy and more recently to ALS (51,52). There is some debate whether the defects resulting from mutations in *MATR3* are primarily myogenic, neuronal or a combination of both (52,99–101); however, the function of MATR3 in muscle cells had not been examined prior to this study.

We demonstrate that MATR3, like PABPN1, regulates key myogenic transcripts and is required for proliferation and proper differentiation of primary mouse myoblasts, potentially indicating that mutations in *MATR3* could underlie muscle defects. While MATR3 does not appear to be essential for bulk poly (A) tail length control (Figure 5), MATR3 does regulate transcripts and steps of post-transcriptional processing in common with PABPN1 (Figures 6 and 7A). Previous microarray analysis of transcripts affected by depletion of MATR3 in HeLa cells identified a major regulatory role for MATR3 in alternative splicing (97). While a majority of the changes reported in the study were observed in the splicing of cassette exons, a significant change in a number of terminal exons and retained introns was also observed. Given the interplay between terminal exon splicing and the cleavage/polyadenylation machinery and the involvement of PABPN1 in alternative polyadenylation and processing of retained introns (10,11,65) we investigated the affect of MATR3 on these processes. With respect to polyadenylation, depletion of MATR3 results in a shortening of the *Tmod1* 3′ UTR through increased utilization of the proximal polyadenylation site (PAS). This effect is opposite to the lengthening of the *Tmod1* 3′ UTR observed upon depletion of PABPN1 from primary myoblasts. The original experiments that identified *Tmod1* as a target for PABPN1-mediated alternative polyadenylation (11), reported a shortening of the 3′ UTR in response to PABPN1 depletion. The difference in the effect observed in this study on 3′ UTR length in response to PABPN1 depletion could be a result of the inherent differences in C2C12 muscle cell lines previously used (11), compared to primary myoblasts used in this study. Indeed, global 3′-end sequencing of RNA obtained from muscles of an OPMD mouse model demonstrated both shortening and lengthening of 3′ UTRs of transcripts when compared to wildtype mice, suggesting their regulation could be context-dependent (41).

Recent studies reveal that PABPN1 is required for polyadenylation and RNA exosome-mediated degradation of transcripts containing retained introns (65,102). PABPN1 utilizes intron retention as a mechanism to auto-regulate levels of its own transcript (14). Binding of PABPN1 inhibits SFRS10-mediated splicing of a terminal intron in the *PABPN1* transcript, such that the intron-containing transcript is subsequently degraded by the RNA-exosome (14). This result suggests a model wherein interplay between PABPN1 and splicing factors could determine the fate of transcripts regulated by intron retention. In our study, depletion of either PABPN1 or MATR3 causes a significant accumulation of the *Mat2a* transcript containing a terminal retained intron (Figure 6C), which suggests that both these proteins normally contribute to the processing and/or decay of this intron-containing transcript. Consistent with this finding, splicing of retained introns of a small subset of transcripts was significantly changed by the depletion of MATR3 in HeLa cells (97). Further work will be required to parse out the direct in-

teraction, if any, of PABPN1 and MATR3 with respect to splicing and/or turnover of retained intron containing transcripts. The presence of both concordant and discordant effects of the depletion of PABPN1 and MATR3 on RNA processing suggests that the nature of interaction between these two proteins could be transcript and context-specific.

Beyond a function in RNA splicing and stability, MATR3 has been implicated in the nuclear retention of A to I (Adenosine to Inosine) edited RNAs (40). RNA editing by the enzyme ADAR (Adenosine deaminase acting on RNA) occurs in paraspeckles (72), which are formed on a *Neat1* scaffold (37–39) and contain RNA binding proteins such as SFPQ and NONO (103–105). *Neat1* levels increase over the course of myoblast differentiation, which raises the possibility, that *Neat1* and by extension paraspeckles may be critical for normal muscle cell function. Past experiments have established a role for PABPN1 in the RNA exosome-mediated turnover of the polyadenylated form of *Neat1*, as the levels of *Neat1* are significantly increased in cells depleted of PABPN1 (16). We present evidence that, like PABPN1, MATR3 binds to and regulates *Neat1* in muscle cells (Figure 7). While previous studies have characterized the molecular mechanisms through which PABPN1 regulates *Neat1*, our analysis establishes PABPN1 and MATR3 as regulators of paraspeckle morphology and function in both murine and human myoblasts.

To establish an *in vivo* paradigm, we examined paraspeckle morphology in muscles obtained from an OPMD mouse model expressing endogenous levels of alanine-expanded PABPN1. These mice show altered paraspeckle protein distribution *in vivo* (Figure 7H). Alanine repeats such as those present in PABPN1 can modulate the intranuclear distribution of the splicing regulator RBM4 between speckles and paraspeckles (106). Perhaps, the pathological aggregates associated with alanine-expanded PABPN1 could alter proteins associated with paraspeckles and result in dysfunction. Furthermore, MATR3 contains an intrinsically disordered domain that predisposes this protein to recruitment into pathological aggregates such as those formed by ALS-associated TDP43 and FUS (107). Although the aggregates formed by alanine-expanded PABPN1 are not the same as those formed by prion-like domains present in TDP43 and FUS, they could be sufficient to sequester MATR3. The precise function of paraspeckles in muscle cells and the direct contribution of disrupted RNA editing if any to OPMD pathogenesis will require further investigation.

Our present work identifies novel protein interactions of PABPN1 in skeletal muscle providing potential clues to yet uncharacterized functions of PABPN1 in muscle biology. The identified interactors could also represent proteins that are susceptible to a loss of function by aggregation with alanine-expanded PABPN1 in OPMD. Further work will be required to compare the protein binding partners of wild-type PABPN1 and alanine-expanded PABPN1 in muscle cells and assess if differential protein-protein interactions contribute to OPMD pathology.

SUPPLEMENTARY DATA

Supplementary Data are available at NAR Online.

ACKNOWLEDGEMENTS

This study was supported in part by the Emory Integrated Genomics Core (EIGC), which is subsidized by the Emory University School of Medicine and is one of the Emory Integrated Core Facilities. Proteomic analysis was performed by the Emory University School of Medicine Integrated Proteomics Core. We thank Dr Kishore Kumar Jella for help with image acquisition. The content is solely the responsibility of the authors and does not necessarily reflect the official views of the National Institutes of Health.

FUNDING

National Institutes of Health [5RO1AR06198705 to A.H.C. and G.K.P., 5F32AR06827 to K.E.V.]; Muscular Dystrophy Association [255856 to A.B. and 422006 to A.H.C.]. Funding for open access charge: National Institutes of Health.
Conflict of interest statement. None declared.

REFERENCES

1. Verkerk,A.J., Pieretti,M., Sutcliffe,J.S., Fu,Y.H., Kuhl,D.P., Pizzuti,A., Reiner,O., Richards,S., Victoria,M.F., Zhang,F.P. *et al.* (1991) Identification of a gene (FMR-1) containing a CGG repeat coincident with a breakpoint cluster region exhibiting length variation in fragile X syndrome. *Cell*, **65**, 905–914.
2. Pak,C., Garshasbi,M., Kahrizi,K., Gross,C., Apponi,L.H., Noto,J.J., Kelly,S.M., Leung,S.W., Tzschach,A., Behjati,F. *et al.* (2011) Mutation of the conserved polyadenosine RNA binding protein, ZC3H14/dNab2, impairs neural function in Drosophila and humans. *Proc. Natl. Acad. Sci. U.S.A.*, **108**, 12390–12395.
3. Ling,S.C., Polymenidou,M. and Cleveland,D.W. (2013) Converging mechanisms in ALS and FTD: disrupted RNA and protein homeostasis. *Neuron*, **79**, 416–438.
4. Liquori,C.L., Ricker,K., Moseley,M.L., Jacobsen,J.F., Kress,W., Naylor,S.L., Day,J.W. and Ranum,L.P. (2001) Myotonic dystrophy type 2 caused by a CCTG expansion in intron 1 of ZNF9. *Science*, **293**, 864–867.
5. Brais,B., Bouchard,J.P., Xie,Y.G., Rochefort,D.L., Chretien,N., Tome,F.M., Lafreniere,R.G., Rommens,J.M., Uyama,E., Nohira,O. *et al.* (1998) Short GCG expansions in the PABP2 gene cause oculopharyngeal muscular dystrophy. *Nat. Genet.*, **18**, 164–167.
6. Wahle,E. (1991) A novel poly(A)-binding protein acts as a specificity factor in the second phase of messenger RNA polyadenylation. *Cell*, **66**, 759–768.
7. Kerwitz,Y., Kuhn,U., Lilie,H., Knoth,A., Scheuermann,T., Friedrich,H., Schwarz,E. and Wahle,E. (2003) Stimulation of poly(A) polymerase through a direct interaction with the nuclear poly(A) binding protein allosterically regulated by RNA. *EMBO J.*, **22**, 3705–3714.
8. Kuhn,U., Gundel,M., Knoth,A., Kerwitz,Y., Rudel,S. and Wahle,E. (2009) Poly(A) tail length is controlled by the nuclear poly(A)-binding protein regulating the interaction between poly(A) polymerase and the cleavage and polyadenylation specificity factor. *J. Biol. Chem.*, **284**, 22803–22814.
9. Apponi,L.H., Leung,S.W., Williams,K.R., Valentini,S.R., Corbett,A.H. and Pavlath,G.K. (2009) Loss of nuclear poly(A)-binding protein 1 causes defects in myogenesis and mRNA biogenesis. *Hum. Mol. Genet.*, **19**, 1058–1065.
10. Jenal,M., Elkon,R., Loayza-Puch,F., van Haaften,G., Kuhn,U., Menzies,F.M., Oude Vrielink,J.A., Bos,A.J., Drost,J., Rooijers,K. *et al.* (2012) The poly(A)-binding protein nuclear 1 suppresses alternative cleavage and polyadenylation sites. *Cell*, **149**, 538–553.
11. de Klerk,E., Venema,A., Anvar,S.Y., Goeman,J.J., Hu,O., den Dunnen,J.T., van der Maarel,S.M., Raz,V. and t Hoen,P.A. (2012) Poly(A) binding protein nuclear 1 levels affect alternative polyadenylation. *Nucleic Acids Res.*
12. Abbassi-Daloii,T., Yousefi,S., de Klerk,E., Grossouw,L., Riaz,M., t Hoen,P.A.C. and Raz,V. (2017) An alanine expanded PABPN1

causes increased utilization of intronic polyadenylation sites. *NPJ Aging Mech. Dis.*, **3**, 6.
13. Muniz,L., Davidson,L. and West,S. (2015) Poly(A) polymerase and the nuclear Poly(A) binding protein, PABPN1, coordinate the splicing and degradation of a subset of human pre-mRNAs. *Mol. Cell Biol*, **35**, 2218–2230.
14. Nguyen,D., Grenier St-Sauveur,V., Bergeron,D., Dupuis-Sandoval,F., Scott,M.S. and Bachand,F. (2015) A polyadenylation-dependent 3' end maturation pathway is required for the synthesis of the human telomerase RNA. *Cell Rep.*, **13**, 2244–2257.
15. Bresson,S.M. and Conrad,N.K. (2013) The human nuclear poly(a)-binding protein promotes RNA hyperadenylation and decay. *PLoS Genet.*, **9**, e1003893.
16. Beaulieu,Y.B., Kleinman,C.L., Landry-Voyer,A.M., Majewski,J. and Bachand,F. (2012) Polyadenylation-dependent control of long noncoding RNA expression by the poly(a)-binding protein nuclear 1. *PLoS Genet.*, **8**, e1003078.
17. Ishigaki,Y., Li,X., Serin,G. and Maquat,L.E. (2001) Evidence for a pioneer round of mRNA translation: mRNAs subject to nonsense-mediated decay in mammalian cells are bound by CBP80 and CBP20. *Cell*, **106**, 607–617.
18. Apponi,L.H., Corbett,A.H. and Pavlath,G.K. (2013) Control of mRNA stability contributes to low levels of nuclear poly(A) binding protein 1 (PABPN1) in skeletal muscle. *Skelet Muscle*, **3**, 23.
19. Victor,M., Hayes,R. and Adams,R.D. (1962) Oculopharyngeal muscular dystrophy. A familial disease of late life characterized by dysphagia and progressive ptosis of the evelids. *N. Engl. J. Med.*, **267**, 1267–1272.
20. Brais,B., Rouleau,G.A., Bouchard,J.P., Fardeau,M. and Tome,F.M. (1999) Oculopharyngeal muscular dystrophy. *Semin. Neurol.*, **19**, 59–66.
21. Calado,A., Tome,F.M., Brais,B., Rouleau,G.A., Kuhn,U., Wahle,E. and Carmo-Fonseca,M. (2000) Nuclear inclusions in oculopharyngeal muscular dystrophy consist of poly(A) binding protein 2 aggregates which sequester poly(A) RNA. *Hum. Mol. Genet.*, **9**, 2321–2328.
22. Bao,Y.P., Cook,L.J., O'Donovan,D., Uyama,E. and Rubinsztein,D.C. (2002) Mammalian, yeast, bacterial, and chemical chaperones reduce aggregate formation and death in a cell model of oculopharyngeal muscular dystrophy. *J. Biol. Chem.*, **277**, 12263–12269.
23. Davies,J.E., Wang,L., Garcia-Oroz,L., Cook,L.J., Vacher,C., O'Donovan,D.G. and Rubinsztein,D.C. (2005) Doxycycline attenuates and delays toxicity of the oculopharyngeal muscular dystrophy mutation in transgenic mice. *Nat. Med.*, **11**, 672–677.
24. Uyama,E., Tsukahara,T., Goto,K., Kurano,Y., Ogawa,M., Kim,Y.J., Uchino,M. and Arahata,K. (2000) Nuclear accumulation of expanded PABP2 gene product in oculopharyngeal muscular dystrophy. *Muscle Nerve*, **23**, 1549–1554.
25. Fan,X., Messaed,C., Dion,P., Laganiere,J., Brais,B., Karpati,G. and Rouleau,G.A. (2003) HnRNP A1 and A/B interaction with PABPN1 in oculopharyngeal muscular dystrophy. *Can. J. Neurol. Sci.*, **30**, 244–251.
26. Corbeil-Girard,L.P., Klein,A.F., Sasseville,A.M., Lavoie,H., Dicaire,M.J., Saint-Denis,A., Page,M., Duranceau,A., Codere,F., Bouchard,J.P. *et al.* (2005) PABPN1 overexpression leads to upregulation of genes encoding nuclear proteins that are sequestered in oculopharyngeal muscular dystrophy nuclear inclusions. *Neurobiol. Dis.*, **18**, 551–567.
27. Tavanez,J.P., Bengoechea,R., Berciano,M.T., Lafarga,M., Carmo-Fonseca,M. and Enguita,F.J. (2009) Hsp70 chaperones and type I PRMTs are sequestered at intranuclear inclusions caused by polyalanine expansions in PABPN1. *PLoS One*, **4**, e6418.
28. Riaz,M., Raz,Y., van Putten,M., Paniagua-Soriano,G., Krom,Y.D., Florea,B.I. and Raz,V. (2016) PABPN1-Dependent mRNA Processing Induces Muscle Wasting. *PLoS Genet.*, **12**, e1006031.
29. Davies,J.E., Sarkar,S. and Rubinsztein,D.C. (2008) Wild-type PABPN1 is anti-apoptotic and reduces toxicity of the oculopharyngeal muscular dystrophy mutation. *Hum. Mol. Genet.*, **17**, 1097–1108.
30. Kim,Y.J., Noguchi,S., Hayashi,Y.K., Tsukahara,T., Shimizu,T. and Arahata,K. (2001) The product of an oculopharyngeal muscular dystrophy gene, poly(A)-binding protein 2, interacts with SKIP and stimulates muscle-specific gene expression. *Hum. Mol. Genet.*, **10**, 1129–1139.
31. Tavanez,J.P., Calado,P., Braga,J., Lafarga,M. and Carmo-Fonseca,M. (2005) In vivo aggregation properties of the nuclear poly(A)-binding protein PABPN1. *RNA*, **11**, 752–762.
32. Belgrader,P., Dey,R. and Berezney,R. (1991) Molecular cloning of matrin 3. A 125-kilodalton protein of the nuclear matrix contains an extensive acidic domain. *J. Biol. Chem.*, **266**, 9893–9899.
33. Zeitz,M.J., Malyavantham,K.S., Seifert,B. and Berezney,R. (2009) Matrin 3: chromosomal distribution and protein interactions. *J. Cell Biochem.*, **108**, 125–133.
34. Salton,M., Lerenthal,Y., Wang,S.Y., Chen,D.J. and Shiloh,Y. (2010) Involvement of Matrin 3 and SFPQ/NONO in the DNA damage response. *Cell Cycle*, **9**, 1568–1576.
35. Yedavalli,V.S. and Jeang,K.T. (2011) Matrin 3 is a co-factor for HIV-1 Rev in regulating post-transcriptional viral gene expression. *Retrovirology*, **8**, 61.
36. Kula,A., Guerra,J., Knezevich,A., Kleva,D., Myers,M.P. and Marcello,A. (2011) Characterization of the HIV-1 RNA associated proteome identifies Matrin 3 as a nuclear cofactor of Rev function. *Retrovirology*, **8**, 60.
37. Sasaki,Y.T., Ideue,T., Sano,M., Mituyama,T. and Hirose,T. (2009) MENepsilon/beta noncoding RNAs are essential for structural integrity of nuclear paraspeckles. *Proc. Natl. Acad. Sci. U.S.A.*, **106**, 2525–2530.
38. Clemson,C.M., Hutchinson,J.N., Sara,S.A., Ensminger,A.W., Fox,A.H., Chess,A. and Lawrence,J.B. (2009) An architectural role for a nuclear noncoding RNA: NEAT1 RNA is essential for the structure of paraspeckles. *Mol. Cell*, **33**, 717–726.
39. Bond,C.S. and Fox,A.H. (2009) Paraspeckles: nuclear bodies built on long noncoding RNA. *J. Cell Biol.*, **186**, 637–644.
40. Zhang,Z. and Carmichael,G.G. (2001) The fate of dsRNA in the nucleus: a p54(nrb)-containing complex mediates the nuclear retention of promiscuously A-to-I edited RNAs. *Cell*, **106**, 465–475.
41. Vest,K.E., Phillips,B.L., Banerjee,A., Apponi,L.H., Dammer,E.B., Xu,W., Zheng,D., Yu,J., Tian,B., Pavlath,G.K. *et al.* (2017) Novel mouse models of oculopharyngeal muscular dystrophy (OPMD) reveal early onset mitochondrial defects and suggest loss of PABPN1 may contribute to pathology. *Hum. Mol. Genet*.
42. Wittig,I., Braun,H.P. and Schagger,H. (2006) Blue native PAGE. *Nat. Protoc.*, **1**, 418–428.
43. Aad,G., Abbott,B., Abdallah,J., Abdinov,O., Aben,R., Abolins,M., AbouZeid,O.S., Abramowicz,H., Abreu,H., Abreu,R. *et al.* (2015) Combined Measurement of the Higgs Boson Mass in pp Collisions at sqrt[s] = 7 and 8 TeV with the ATLAS and CMS Experiments. *Phys. Rev. Lett.*, **114**, 191803.
44. Griffin,C.A., Kafadar,K.A. and Pavlath,G.K. (2009) MOR23 promotes muscle regeneration and regulates cell adhesion and migration. *Dev. Cell*, **17**, 649–661.
45. Pichavant,C. and Pavlath,G.K. (2014) Incidence and severity of myofiber branching with regeneration and aging. *Skelet. Muscle*, **4**, 9.
46. Ule,J., Jensen,K., Mele,A. and Darnell,R.B. (2005) CLIP: a method for identifying protein-RNA interaction sites in living cells. *Methods*, **37**, 376–386.
47. Bondesen,B.A., Mills,S.T., Kegley,K.M. and Pavlath,G.K. (2004) The COX-2 pathway is essential during early stages of skeletal muscle regeneration. *Am. J. Physiol. Cell Physiol.*, **287**, C475–C483.
48. Cutler,A.A., Dammer,E.B., Doung,D.M., Seyfried,N.T., Corbett,A.H. and Pavlath,G.K. (2017) Biochemical isolation of myonuclei employed to define changes to the myonuclear proteome that occur with aging. *Aging Cell*, **16**, 738–749.
49. White,M.K., Johnson,E.M. and Khalili,K. (2009) Multiple roles for Puralpha in cellular and viral regulation. *Cell Cycle*, **8**, 1–7.
50. Koseki,T., Inohara,N., Chen,S. and Nunez,G. (1998) ARC, an inhibitor of apoptosis expressed in skeletal muscle and heart that interacts selectively with caspases. *Proc. Natl. Acad. Sci. U.S.A.*, **95**, 5156–5160.
51. Senderek,J., Garvey,S.M., Krieger,M., Guergueltcheva,V., Urtizberea,A., Roos,A., Elbracht,M., Stendel,C., Tournev,I., Mihailova,V. *et al.* (2009) Autosomal-dominant distal myopathy associated with a recurrent missense mutation in the gene encoding the nuclear matrix protein, matrin 3. *Am. J. Hum. Genet.*, **84**, 511–518.

52. Johnson,J.O., Pioro,E.P., Boehringer,A., Chia,R., Feit,H., Renton,A.E., Pliner,H.A., Abramzon,Y., Marangi,G., Winborn,B.J. *et al.* (2014) Mutations in the Matrin 3 gene cause familial amyotrophic lateral sclerosis. *Nat. Neurosci.*, **17**, 664–666.
53. Salton,M., Elkon,R., Borodina,T., Davydov,A., Yaspo,M.L., Halperin,E. and Shiloh,Y. (2011) Matrin 3 binds and stabilizes mRNA. *PLoS One*, **6**, e23882.
54. Bland,C.S., Wang,E.T., Vu,A., David,M.P., Castle,J.C., Johnson,J.M., Burge,C.B. and Cooper,T.A. (2010) Global regulation of alternative splicing during myogenic differentiation. *Nucleic Acids Res.*, **38**, 7651–7664.
55. Li,W., You,B., Hoque,M., Zheng,D., Luo,W., Ji,Z., Park,J.Y., Gunderson,S.I., Kalsotra,A., Manley,J.L. *et al.* (2015) Systematic profiling of poly(A)+ transcripts modulated by core 3' end processing and splicing factors reveals regulatory rules of alternative cleavage and polyadenylation. *PLoS Genet.*, **11**, e1005166.
56. Pilaz,L.J. and Silver,D.L. (2015) Post-transcriptional regulation in corticogenesis: how RNA-binding proteins help build the brain. *Wiley Interdiscip. Rev. RNA*, **6**, 501–515.
57. Kiebler,M.A., Scheiffele,P. and Ule,J. (2013) What, where, and when: the importance of post-transcriptional regulation in the brain. *Front. Neurosci.*, **7**, 192.
58. Kim,S.H., Shanware,N.P., Bowler,M.J. and Tibbetts,R.S. (2010) Amyotrophic lateral sclerosis-associated proteins TDP-43 and FUS/TLS function in a common biochemical complex to co-regulate HDAC6 mRNA. *J. Biol. Chem.*, **285**, 34097–34105.
59. Chou,C.C., Alexeeva,O.M., Yamada,S., Pribadi,A., Zhang,Y., Mo,B., Williams,K.R., Zarnescu,D.C. and Rossoll,W. (2015) PABPN1 suppresses TDP-43 toxicity in ALS disease models. *Hum. Mol. Genet.*, **24**, 5154–5173.
60. Andres,V. and Walsh,K. (1996) Myogenin expression, cell cycle withdrawal, and phenotypic differentiation are temporally separable events that precede cell fusion upon myogenesis. *J. Cell Biol.*, **132**, 657–666.
61. Berkes,C.A. and Tapscott,S.J. (2005) MyoD and the transcriptional control of myogenesis. *Semin. Cell Dev. Biol.*, **16**, 585–595.
62. Costelli,P., Almendro,V., Figueras,M.T., Reffo,P., Penna,F., Aragno,M., Mastrocola,R., Boccuzzi,G., Busquets,S., Bonelli,G. *et al.* (2007) Modulations of the calcineurin/NF-AT pathway in skeletal muscle atrophy. *Biochim. Biophys. Acta*, **1770**, 1028–1036.
63. Cesana,M., Cacchiarelli,D., Legnini,I., Santini,T., Sthandier,O., Chinappi,M., Tramontano,A. and Bozzoni,I. (2011) A long noncoding RNA controls muscle differentiation by functioning as a competing endogenous RNA. *Cell*, **147**, 358–369.
64. Bentzinger,C.F., Wang,Y.X. and Rudnicki,M.A. (2012) Building muscle: molecular regulation of myogenesis. *Cold Spring Harb. Perspect. Biol.*, **4**, a008342.
65. Bresson,S.M., Hunter,O.V., Hunter,A.C. and Conrad,N.K. (2015) Canonical Poly(A) polymerase activity promotes the decay of a wide variety of mammalian nuclear RNAs. *PLoS Genet.*, **11**, e1005610.
66. Gautheret,D., Poirot,O., Lopez,F., Audic,S. and Claverie,J.M. (1998) Alternate polyadenylation in human mRNAs: a large-scale analysis by EST clustering. *Genome Res.*, **8**, 524–530.
67. Tian,B., Hu,J., Zhang,H. and Lutz,C.S. (2005) A large-scale analysis of mRNA polyadenylation of human and mouse genes. *Nucleic Acids Res.*, **33**, 201–212.
68. LeGros,H.L. Jr, Halim,A.B., Geller,A.M. and Kotb,M. (2000) Cloning, expression, and functional characterization of the beta regulatory subunit of human methionine adenosyltransferase (MAT II). *J. Biol. Chem.*, **275**, 2359–2366.
69. Prasanth,K.V., Prasanth,S.G., Xuan,Z., Hearn,S., Freier,S.M., Bennett,C.F., Zhang,M.Q. and Spector,D.L. (2005) Regulating gene expression through RNA nuclear retention. *Cell*, **123**, 249–263.
70. Shav-Tal,Y., Blechman,J., Darzacq,X., Montagna,C., Dye,B.T., Patton,J.G., Singer,R.H. and Zipori,D. (2005) Dynamic sorting of nuclear components into distinct nucleolar caps during transcriptional inhibition. *Mol. Biol. Cell*, **16**, 2395–2413.
71. Naganuma,T., Nakagawa,S., Tanigawa,A., Sasaki,Y.F., Goshima,N. and Hirose,T. (2012) Alternative 3'-end processing of long noncoding RNA initiates construction of nuclear paraspeckles. *EMBO J.*, **31**, 4020–4034.
72. Chen,L.L. and Carmichael,G.G. (2009) Altered nuclear retention of mRNAs containing inverted repeats in human embryonic stem cells: functional role of a nuclear noncoding RNA. *Mol. Cell*, **35**, 467–478.
73. Yoon,J.H., De,S., Srikantan,S., Abdelmohsen,K., Grammatikakis,I., Kim,J., Kim,K.M., Noh,J.H., White,E.J., Martindale,J.L. *et al.* (2014) PAR-CLIP analysis uncovers AUF1 impact on target RNA fate and genome integrity. *Nat. Commun.*, **5**, 5248.
74. Afonina,E., Stauber,R. and Pavlakis,G.N. (1998) The human poly(A)-binding protein 1 shuttles between the nucleus and the cytoplasm. *J. Biol. Chem.*, **273**, 13015–13021.
75. Gorgoni,B. and Gray,N.K. (2004) The roles of cytoplasmic poly(A)-binding proteins in regulating gene expression: a developmental perspective. *Brief Funct. Genomic Proteomic*, **3**, 125–141.
76. Burgess,H.M., Richardson,W.A., Anderson,R.C., Salaun,C., Graham,S.V. and Gray,N.K. (2011) Nuclear relocalisation of cytoplasmic poly(A)-binding proteins PABP1 and PABP4 in response to UV irradiation reveals mRNA-dependent export of metazoan PABPs. *J. Cell Sci.*, **124**, 3344–3355.
77. Behm-Ansmant,I., Gatfield,D., Rehwinkel,J., Hilgers,V. and Izaurralde,E. (2007) A conserved role for cytoplasmic poly(A)-binding protein 1 (PABPC1) in nonsense-mediated mRNA decay. *EMBO J.*, **26**, 1591–1601.
78. Imataka,H., Gradi,A. and Sonenberg,N. (1998) A newly identified N-terminal amino acid sequence of human eIF4G binds poly(A)-binding protein and functions in poly(A)-dependent translation. *EMBO J.*, **17**, 7480–7489.
79. Hosoda,N., Lejeune,F. and Maquat,L.E. (2006) Evidence that poly(A) binding protein C1 binds nuclear pre-mRNA poly(A) tails. *Mol. Cell Biol.*, **26**, 3085–3097.
80. Kini,H.K., Kong,J. and Liebhaber,S.A. (2014) Cytoplasmic poly(A) binding protein C4 serves a critical role in erythroid differentiation. *Mol. Cell. Biol.*, **34**, 1300–1309.
81. Bhattacharjee,R.B. and Bag,J. (2012) Depletion of nuclear poly(A) binding protein PABPN1 produces a compensatory response by cytoplasmic PABP4 and PABP5 in cultured human cells. *PLoS One*, **7**, e53036.
82. Chen,H.H., Chang,J.G., Lu,R.M., Peng,T.Y. and Tarn,W.Y. (2008) The RNA binding protein hnRNP Q modulates the utilization of exon 7 in the survival motor neuron 2 (SMN2) gene. *Mol. Cell. Biol.*, **28**, 6929–6938.
83. Zarnack,K., Konig,J., Tajnik,M., Martincorena,I., Eustermann,S., Stevant,I., Reyes,A., Anders,S., Luscombe,N.M. and Ule,J. (2013) Direct competition between hnRNP C and U2AF65 protects the transcriptome from the exonization of Alu elements. *Cell*, **152**, 453–466.
84. Nasrin,F., Rahman,M.A., Masuda,A., Ohe,K., Takeda,J. and Ohno,K. (2014) HnRNP C, YB-1 and hnRNP L coordinately enhance skipping of human MUSK exon 10 to generate a Wnt-insensitive MuSK isoform. *Sci. Rep.*, **4**, 6841.
85. Shetty,S. (2005) Regulation of urokinase receptor mRNA stability by hnRNP C in lung epithelial cells. *Mol. Cell Biochem.*, **272**, 107–118.
86. Bannai,H., Fukatsu,K., Mizutani,A., Natsume,T., Iemura,S., Ikegami,T., Inoue,T. and Mikoshiba,K. (2004) An RNA-interacting protein, SYNCRIP (heterogeneous nuclear ribonuclear protein Q1/NSAP1) is a component of mRNA granule transported with inositol 1,4,5-trisphosphate receptor type 1 mRNA in neuronal dendrites. *J. Biol. Chem.*, **279**, 53427–53434.
87. Lee,E.K., Kim,H.H., Kuwano,Y., Abdelmohsen,K., Srikantan,S., Subaran,S.S., Gleichmann,M., Mughal,M.R., Martindale,J.L., Yang,X. *et al.* (2010) hnRNP C promotes APP translation by competing with FMRP for APP mRNA recruitment to P bodies. *Nat. Struct. Mol. Biol.*, **17**, 732–739.
88. Klein,P., Oloko,M., Roth,F., Montel,V., Malerba,A., Jarmin,S., Gidaro,T., Popplewell,L., Perie,S., Lacau St Guily,J. *et al.* (2016) Nuclear poly(A)-binding protein aggregates misplace a pre-mRNA outside of SC35 speckle causing its abnormal splicing. *Nucleic Acids Res.*, **44**, 10929–10945.
89. Ekhterae,D., Lin,Z., Lundberg,M.S., Crow,M.T., Brosius,F.C. 3rd and Nunez,G. (1999) ARC inhibits cytochrome c release from mitochondria and protects against hypoxia-induced apoptosis in heart-derived H9c2 cells. *Circ. Res.*, **85**, e70–77.
90. Heikaus,S., Kempf,T., Mahotka,C., Gabbert,H.E. and Ramp,U. (2008) Caspase-8 and its inhibitors in RCCs in vivo: the prominent role of ARC. *Apoptosis*, **13**, 938–949.

91. Mitchell,A.S., Smith,I.C., Gamu,D., Donath,S., Tupling,A.R. and Quadrilatero,J. (2015) Functional, morphological, and apoptotic alterations in skeletal muscle of ARC deficient mice. *Apoptosis*, **20**, 310–326.
92. Davies,J.E. and Rubinsztein,D.C. (2011) Over-expression of BCL2 rescues muscle weakness in a mouse model of oculopharyngeal muscular dystrophy. *Hum. Mol. Genet.*, **20**, 1154–1163.
93. Graebsch,A., Roche,S. and Niessing,D. (2009) X-ray structure of Pur-alpha reveals a Whirly-like fold and an unusual nucleic-acid binding surface. *Proc. Natl. Acad. Sci. U.S.A.*, **106**, 18521–18526.
94. Darbinian,N., Cui,J., Basile,A., Del Valle,L., Otte,J., Miklossy,J., Sawaya,B.E., Amini,S., Khalili,K. and Gordon,J. (2008) Negative regulation of AbetaPP gene expression by pur-alpha. *J. Alzheimers Dis.*, **15**, 71–82.
95. Johnson,E.M., Kinoshita,Y., Weinreb,D.B., Wortman,M.J., Simon,R., Khalili,K., Winckler,B. and Gordon,J. (2006) Role of Pur alpha in targeting mRNA to sites of translation in hippocampal neuronal dendrites. *J. Neurosci. Res.*, **83**, 929–943.
96. Di Salvio,M., Piccinni,V., Gerbino,V., Mantoni,F., Camerini,S., Lenzi,J., Rosa,A., Chellini,L., Loreni,F., Carri,M.T. *et al.* (2015) Pur-alpha functionally interacts with FUS carrying ALS-associated mutations. *Cell Death Dis.*, **6**, e1943.
97. Coelho,M.B., Attig,J., Bellora,N., Konig,J., Hallegger,M., Kayikci,M., Eyras,E., Ule,J. and Smith,C.W. (2015) Nuclear matrix protein Matrin3 regulates alternative splicing and forms overlapping regulatory networks with PTB. *EMBO J.*, **34**, 653–668.
98. Depreux,F.F., Puckelwartz,M.J., Augustynowicz,A., Wolfgeher,D., Labno,C.M., Pierre-Louis,D., Cicka,D., Kron,S.J., Holaska,J. and McNally,E.M. (2015) Disruption of the lamin A and matrin-3 interaction by myopathic LMNA mutations. *Hum. Mol. Genet.*, **24**, 4284–4295.
99. Muller,T.J., Kraya,T., Stoltenburg-Didinger,G., Hanisch,F., Kornhuber,M., Stoevesandt,D., Senderek,J., Weis,J., Baum,P., Deschauer,M. *et al.* (2014) Phenotype of matrin-3-related distal myopathy in 16 German patients. *Ann. Neurol.*, **76**, 669–680.
100. Moloney,C., Rayaprolu,S., Howard,J., Fromholt,S., Brown,H., Collins,M., Cabrera,M., Duffy,C., Siemienski,Z., Miller,D. *et al.* (2016) Transgenic mice overexpressing the ALS-linked protein Matrin 3 develop a profound muscle phenotype. *Acta Neuropathol. Commun.*, **4**, 122.
101. Yamashita,S., Mori,A., Nishida,Y., Kurisaki,R., Tawara,N., Nishikami,T., Misumi,Y., Ueyama,H., Imamura,S., Higuchi,Y. *et al.* (2015) Clinicopathological features of the first Asian family having vocal cord and pharyngeal weakness with distal myopathy due to a MATR3 mutation. *Neuropathol. Appl. Neurobiol.*, **41**, 391–398.
102. Meola,N., Domanski,M., Karadoulama,E., Chen,Y., Gentil,C., Pultz,D., Vitting-Seerup,K., Lykke-Andersen,S., Andersen,J.S., Sandelin,A. *et al.* (2016) Identification of a nuclear exosome decay pathway for processed transcripts. *Mol. Cell*, **64**, 520–533.
103. Fox,A.H., Lam,Y.W., Leung,A.K., Lyon,C.E., Andersen,J., Mann,M. and Lamond,A.I. (2002) Paraspeckles: a novel nuclear domain. *Curr. Biol.*, **12**, 13–25.
104. Fox,A.H., Bond,C.S. and Lamond,A.I. (2005) P54nrb forms a heterodimer with PSP1 that localizes to paraspeckles in an RNA-dependent manner. *Mol. Biol. Cell*, **16**, 5304–5315.
105. Knott,G.J., Bond,C.S. and Fox,A.H. (2016) The DBHS proteins SFPQ, NONO and PSPC1: a multipurpose molecular scaffold. *Nucleic Acids Res.*, **44**, 3989–4004.
106. Chang,S.H., Chang,W.L., Lu,C.C. and Tarn,W.Y. (2014) Alanine repeats influence protein localization in splicing speckles and paraspeckles. *Nucleic Acids Res.*, **42**, 13788–13798.
107. King,O.D., Gitler,A.D. and Shorter,J. (2012) The tip of the iceberg: RNA-binding proteins with prion-like domains in neurodegenerative disease. *Brain Res.*, **1462**, 61–80.